Free Oscillations and Surface Waves

Gabi Laske

Institute of Geophysics and Planetary Physics,
SIO, UC San Diego

this is an annotated version of the lecture given at the July 2012 CIDER summer school at KITP, UC Santa Barbara.

Some slides are duplicated here to provide more space for annotations.

For questions, please contact me at glaske@ucsd.edu

my website is: http://igppweb.ucsd.edu/~gabi

Reference:

Laske, G. and Widmer-Schnidrig, R., Normal Mode & Surface Wave Observations. in: "Treatise on Geophysics, Volume 1: Seismology and Structure of the Earth", Vol. 1, 67-125, 2007.

to download a pre-print, go to http://igppweb.ucsd.edu/~gabi

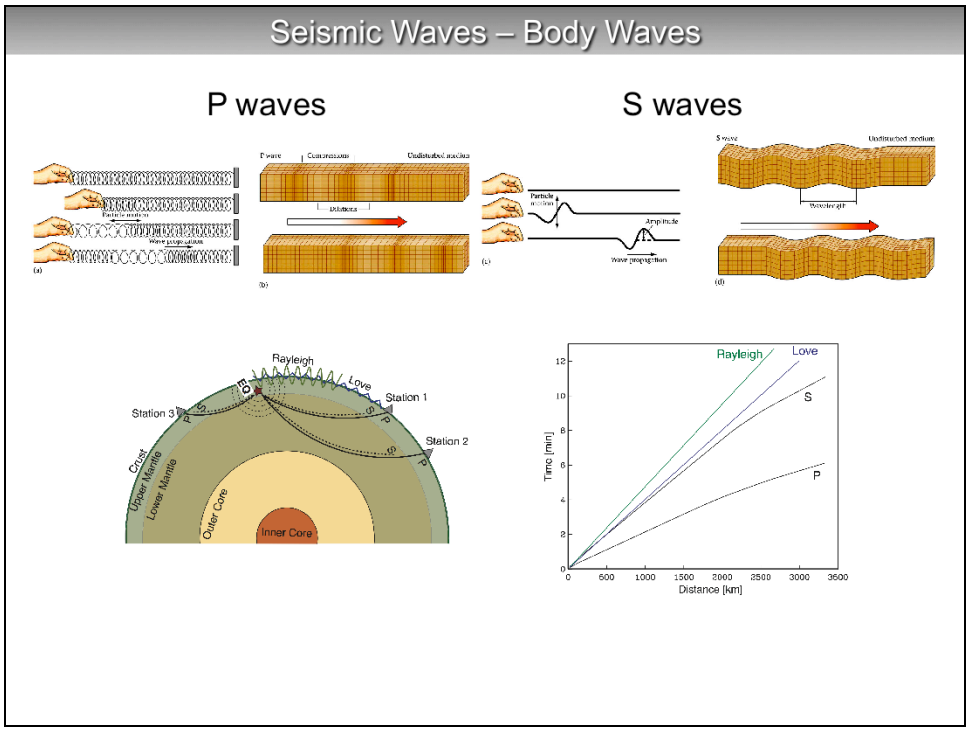

on a finite body such as Earth, seismic waves can be regarded as traveling waves (i.e. a disturbance travels in the medium) or as standing waves, i.e. the body resonates at certain frequencies that are defined by the geometry and internal properties of the body, such as density structure and local variations in compressional and shear velocity.

Traveling and standing waves can be obtained by superposition of the other type, i.e. make normal modes by superimposing body waves and surface waves, or make traveling waves by superposition of normal modes.

The particle motion of compressional waves (P waves) is in the direction of propagation, similar to that of sound waves. The particle motion of shear waves (S waves) is perpendicular to the propagation direction. As with light waves (electromagnetic waves), it is convenient to decompose S waves into two waves, one with purely horizontal polarization (SH) and one perpendicular to that (SV). The VS motion has a horizontal and a vertical component,

and SV waves can transition into P waves and vice versa when refracting and reflecting from interfaces, while SH waves reflect and refract only

into SH waves.

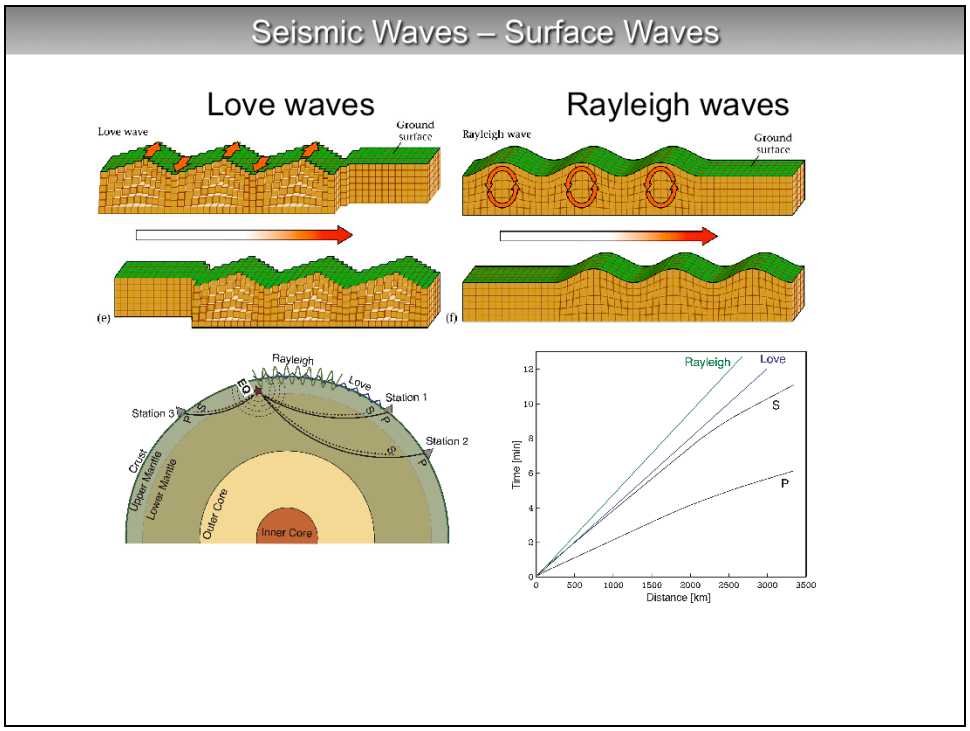

Apart from the two types of body waves that travel through Earth, surface waves propagate relatively slowly along Earth's surface (see travel-time plot in lower right). At short distances, surface waves overlap with shear waves and it is not really possible to distinguish between them. In a widest sense, Love waves can be generated by superposition of SH-polarized shear waves. In the widest sense, Rayleigh waves can be obtained through the superposition of P and SV body waves that are reflected and refracted within Earth's upper layers. The particle motion of surface waves decays exponentially with depth.

In a travel-time plot (lower right), surface-wave times follow a straight line (surface waves travel at a certain speed) while

body-wave times follow a curve (with increasing distance, body waves dove deeper inside Earth, experiencing increased

in velocity).

Rayleigh Waves – Water Surface Waves

- arrive last
- combination of reflected P and S waves
- motion decreases exponentially with depth
- like water waves, but
- retrograde elliptical particle motion

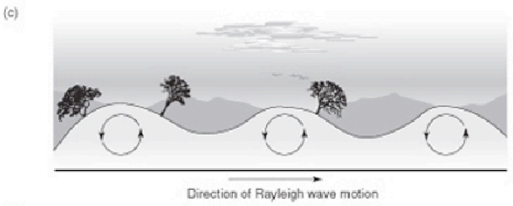

retrograde Rayleigh waves
elliptical particle motion

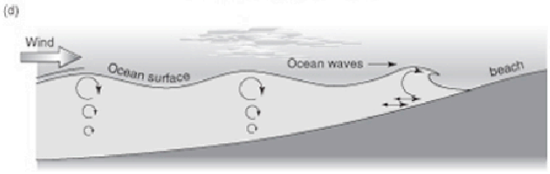

prograde water waves
circular particle motion

BTW: energy transport
but no mass transport

Rayleigh waves are often likened to surface waves in water but there exist fundamental differences. To start with, Rayleigh waves have a shear component, water waves only have compressional components. The particle motion of water waves is circular, that of Rayleigh waves is elliptical. Water waves are prograde, i.e. the sense of particle motion (the upper arc of the particle-motion circle) is in the propagation direction (i.e. away from you). Rayleigh waves are retrograde (the upper arc of the particle motion is against the propagation direction, i.e. toward you).

NB: waves transport energy but not matter. I.e. a tsunami does not really transport debris. The latter is transported by ocean currents.

Debris from the 11 March Tohoku earthquake has now started to arrive at the North American west coast, a little over a year later.

A 3-Component Seismogram

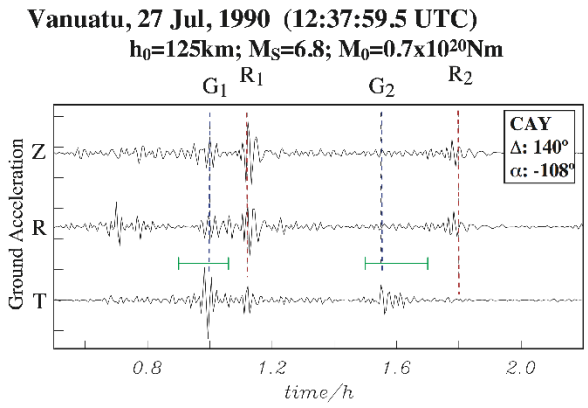

an example of a seismogram: the 27 july 1990 Vanuatu earthquake observed at station CAY (Cayenne, French Guiana).

Source depth: 125 km; surface wave magnitude 6.8; scalar seismic moment (measure for energy released) 0.7 x 10^20 Nm. The earthquake was 140 deg away from the station (epicentral distance) and 108 deg in a westerly direction (back-azimuth -108 deg). Time is from the time of the earthquake.

Three orthogonal seismometers define ground motion in 3-dimensional space: vertical component (Z); radial component (R) which is a horizontal component pointing in the direction to the earthquake; transverse component (T) which is a horizontal component perpendicular to the receiver-source direction (backazimuth).

The largest signal is from the two surface waves (Love on T component). The direct source-to-receiver Love wave is G1 (minor arc, see next slide), while G2 is the Love wave that took the long way around the Earth (major arc). R1 and R2 are the corresponding Rayleigh wave packets on the Z and R components. Signals leading the surface wave trains are body waves. S-waves are often very strong on the R component, while the first-arriving

P-wave typically have small amplitudes (first wiggle on Z-component). Green lines indicate the time window that we would choose for an analysis of the Love wavetrains G1 and G2 We choose windows that include as much as possible of the wavetrain of interest but cutting out as much as possible of the signals we are not interested in..

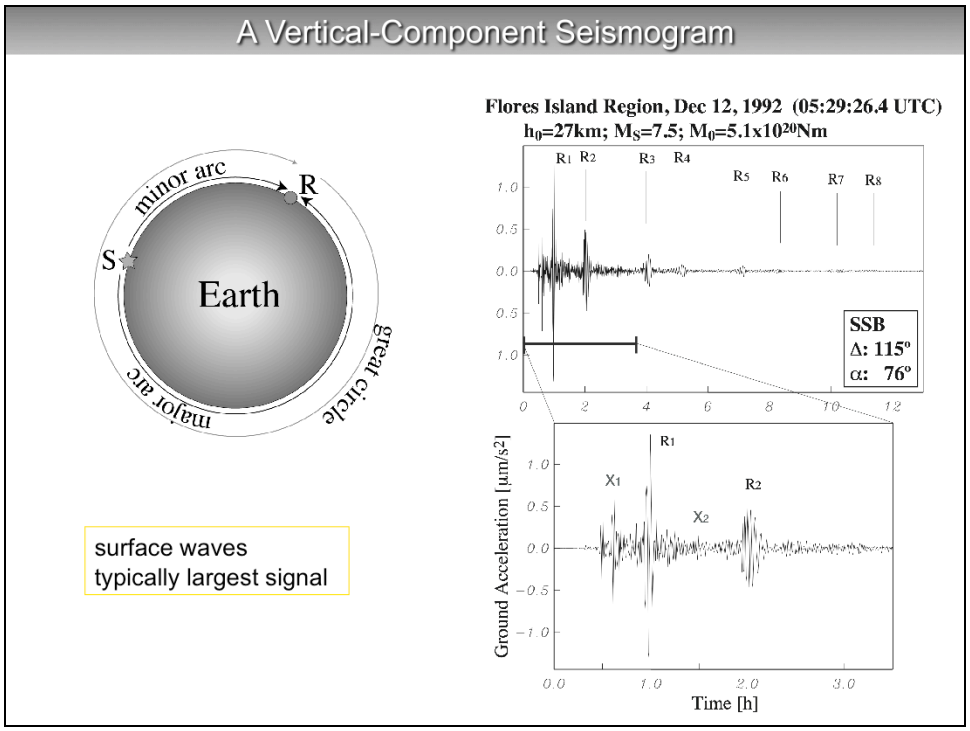

a vertical-component seismogram, now 12-hours long, allowing to see Rayleigh waves that circled the globe several times.

The recording station SSB is Saint Sauveur-Badole in France, at an epicentral distance of 115 deg and receiver-source azimuth of 76 deg.

The source-receiver great circle is the circle on the globe that represents the shortest distance between the source and the receiver.

The nomenclature of surface wave trains is such that odd wave orbit numbers (i.e. R1, R3 …) denote wavetrains that travel in the direction of the minor arc, increasing by 2 for each successive complete circumnavigation of the globe, i.e. R1 is the first minor arc wavetrain. It becomes R3 after it completed a whole circle around the globe and then arriving at the station. Even wave orbit numbers (R2, R4 …) are waves that travel the long way to the station (i.e. in the direction of the major arc). It takes about 3h for surface waves to complete a great circle, e.g. the time difference between R1 and R3 is 3h.

Here, body waves are denoted as X1 and X2. These also bounce off Earth's surface and circle the globe several times (next slide).

In terms of standing waves, Love and Rayleigh wave represent fundamental modes, while the X1 phases make up overtones.

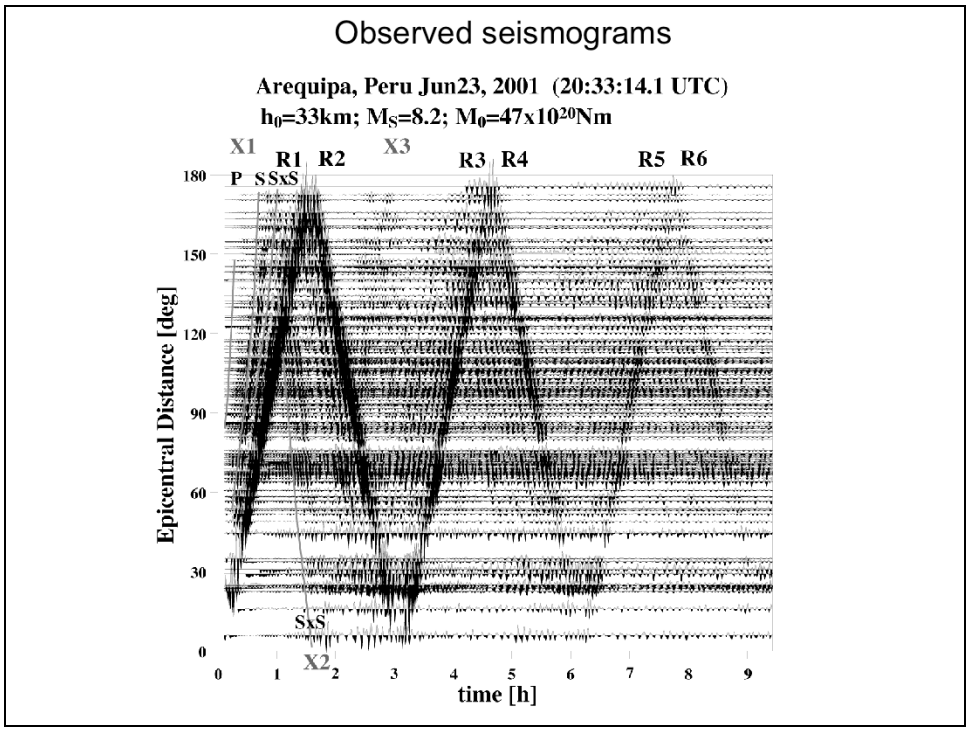

A record section for an earthquake, i.e. recordings of many stations around the globe, sorted by epicentral distance. Within about 20 deg of the source and the antipode, two surface wave trains overlap, i.e. they arrive at the same time, forming a caustic.

At epicentral distances of 90 deg, minor- and major-arc surface wave trains are spaced equally in time. This record section shows how waves propagate on and inside the globe. In the next two slide, we will regard seismograms from a standing wave (resonance vibrations) point of view.

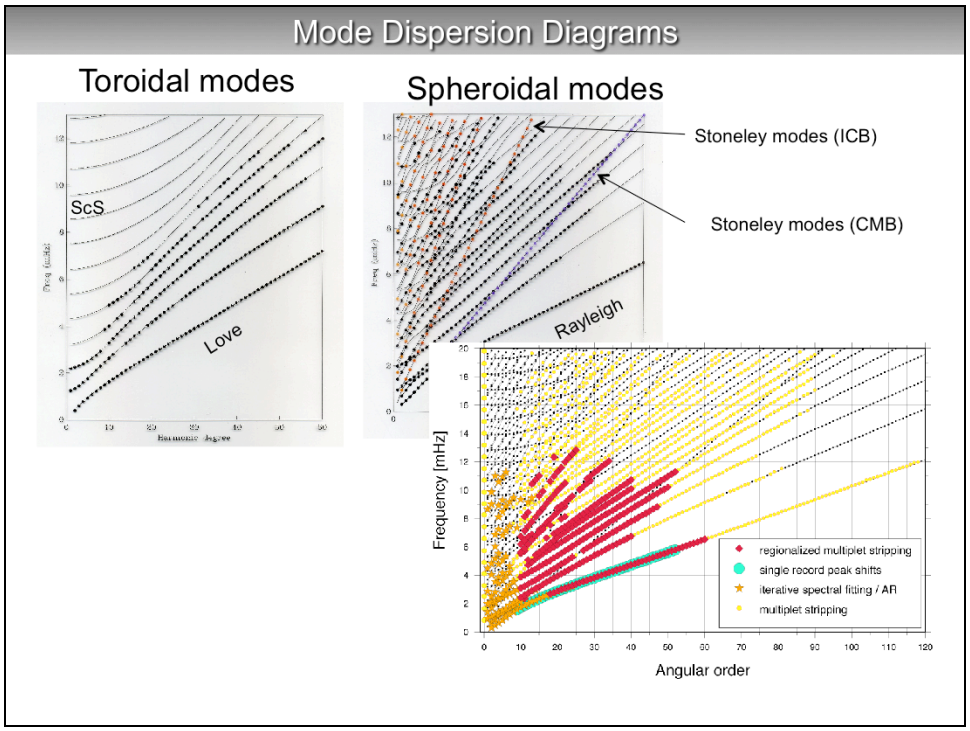

Dispersion diagrams showing the resonance frequencies of Earth, for toroidal mode (purely horizontal, transversely shearing motion and spheroidal modes (compressional motion and horizontally and vertically shearing motion). Since Earth is a finite body, frequencies are discrete, and not a continuum along the frequency (y-axis) and wavenumber (x-axis) axes. The modes are sorted according to mode branch/overtone number.

The diagram for toroidal modes is simple, with mode branches well isolated from each other (dots denote modes that have actually been observed). The lowest branch in the fundamental mode (Love waves).

The diagram for spheroidal modes is much more complicated and only the fundamental mode (Rayleigh waves) is isolated while the other branches approach each other or even cross.

Two mode branches cannot be observed at Earth's surface. These are related to Stoneley modes along the fluid/solid interfaces inside Earth, i.e. the inner-core boundary and the core-mantle boundary. The motion of Stoneley modes decays exponentially away from the boundaries. One way, some individual modes could potentially be observed is if they couple with other modes that are observed at Earth's surface. In this case, the Stoneley mode transfers some of its energy into the observable mode and modulates the frequency of that mode (in principle, the observable change of the frequency of that mode can be used to analyze the Stoneley mode). We use different methods to analyze modes (shown in the color plot).

Modes and Earth Structure

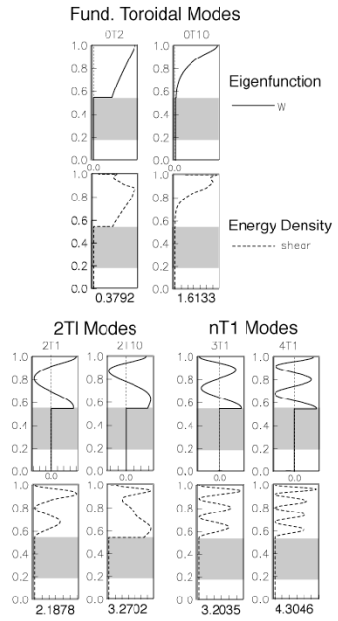

Toroidal Modes

- nTl; n # nodes in W radially
- W=0 in outer core
- inner-core modes not observed

these diagrams show the sensitivity of individual modes to Earth structure, for a spherically averaged Earth. 3-D structure is often included using perturbation theory as changes in vertical structure are much larger than lateral variations.

In each panel, the x-axis is the amplitude of the function and y-axis is normalized Earth radius. Upper white region is the mantle, grey region is the outer core, lower white region is the inner core. Numbers below the diagrams indicate
the frequency (in mHz) of the mode.
For each mode, the top panels show the eigenfunctions, i.e. the integral kernel that is related to treating and solving the wave equation as an eigenvalue problem were the eigenfunctions are the eigenvectors and the mode frequencies the eigenvalues. For toroidal modes, we have one eigenfuction (W) while for spheroidal modes, there are two (V, U). The lower panels show energy densities which can be computed from the eigenfunctions. In terms of how modes sense Earth structure, energy densities are easier to interpret. Toroidal modes have non-zero energy densities only in shear, while for spheroidal modes (next slide) also have non-zerocompressional energy densities. The shear energies are zero in the outer core. Energy densities have to be non-zero at Earth's surface in order for the modes to be observable. Normal modes are also sensitive to variations in Earth's density!

Toroidal modes are named nTl where n denotes the overtone number (n=0 is fundamental mode). Non-zero numbers denote the number of nodes in the eigenfunction. l is the angular order where l-1 describes the number of nodal lines on Earth's surface.
The most basic mode is 0T2 which has a nodal line along the equator, and the "northern" hemisphere rotates in one direction while the "southern" hemisphere rotates in the other.

Modes that only have non-zero energy densities in the inner core are not observed on the surface (unless they couple to observable modes).

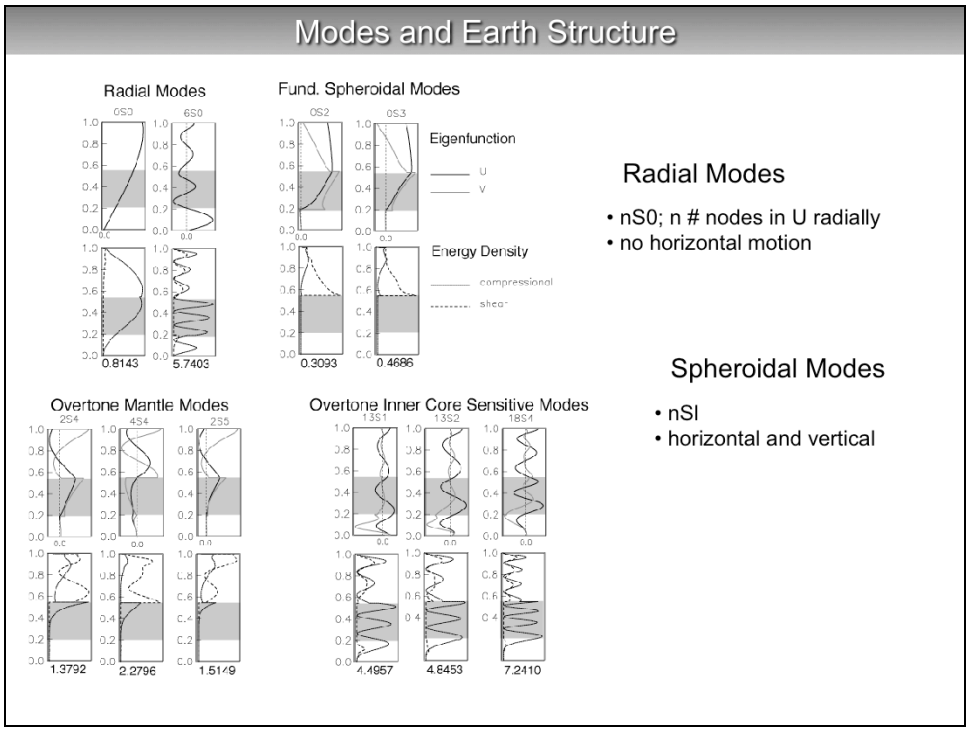

Corresponding diagrams for spheroidal modes. We regard modes that have no horizontal motion separately. These are the radial

modes, and their eigenfunction V is zero. The most basic radial mode is 0S0, the “breathing mode” where Earth’s surface rises

and falls at the same rate everywhere on the globe.

0Sl are the fundamental modes. The most basic mode is the football mode 0S2 that changes in shape like a squeezed football.

Synthetic (Body Wave) Seismograms by Mode Summation

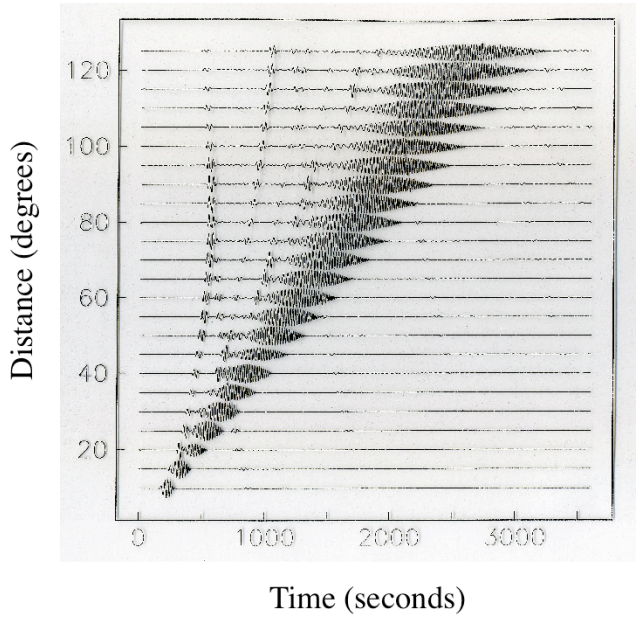

to make the point of traveling wave-standing wave duality, surface waves and also even body waves can be obtained by summing all normal modes. The record section shows

synthetic seismograms computed by mode-summation. Clearly, the traveling surface wave shows up, but

also the earlier-arriving body waves.

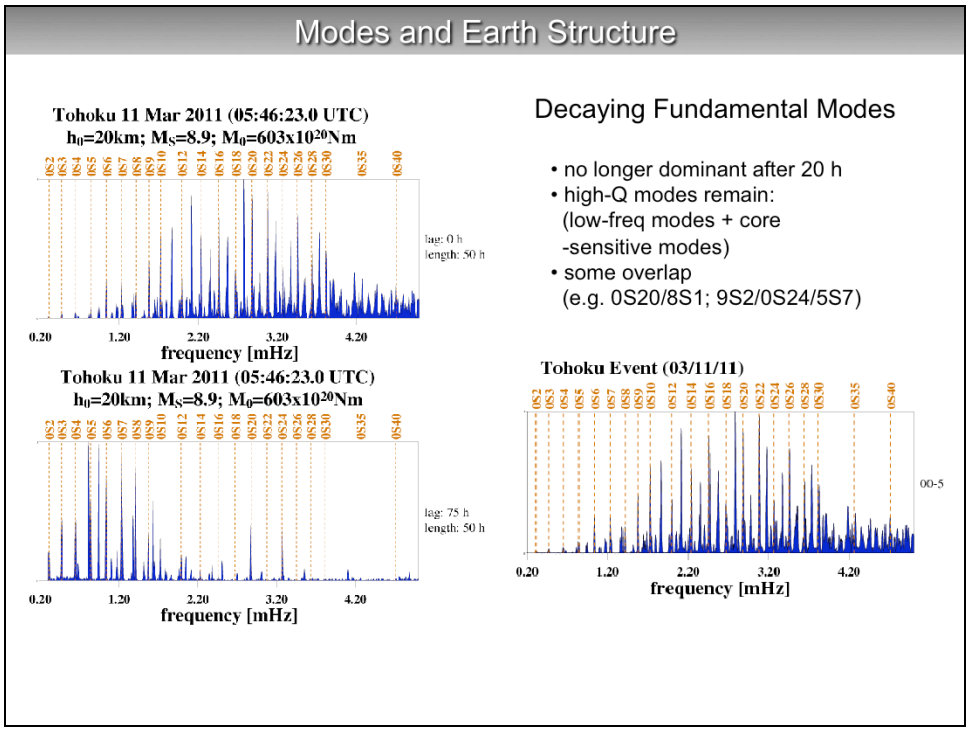

We calculate spectra of seismograms to analyze modes, i.e., in principle, we choose a time window in the seismogram and perform a Fourier Transform. Squared spectra are proportional to the energy content of the seismogram. It should be noted here that Earth's outer core is much less attenuating than the mantle. So core-sensitive modes are high-Q modes (Q is the quality factor and Q=1/q where q is mode attenuation). This means that fundamental modes, which "see" only the mantle, will decay faster as time goes on than core-sensitive modes. And higher-l fundamental modes that "see" only shallower structure, will decay faster than lower-l fundamental modes. A spectrum associated with a time-window early in the time series is dominated by fundamental modes. If we start later and later in the time series, high-Q modes will increase to "survive" in the spectrum (lower left, that shows a spectrum for a window that starts 75 h after the earthquake). Low-l fundamental modes remain. For example, a peak emerges 0s5 and 0s6. This peak belongs to a pair of overtones that have nearly the same frequency 1s3 and 3s1.

NB: the spectra are normalized! In reality, the lower left spectrum is much lower in amplitude than the upper spectrum (lower right was a movie shown in the talk).

In the later spectrum, some peaks remain at fundamental-mode frequencies, e.g. 0S20. These are not really fundamental modes but core-sensitive modes that overlap in frequency with fundamental modes (e.g. 8S1). In the spectrum of a single station, we would not be able to distinguish between modes. But by stacking spectra observed globally in certain ways, we can find out which of the modes we are observing here. To do this, we need to know what the oscillations look like laterally, see next slide.

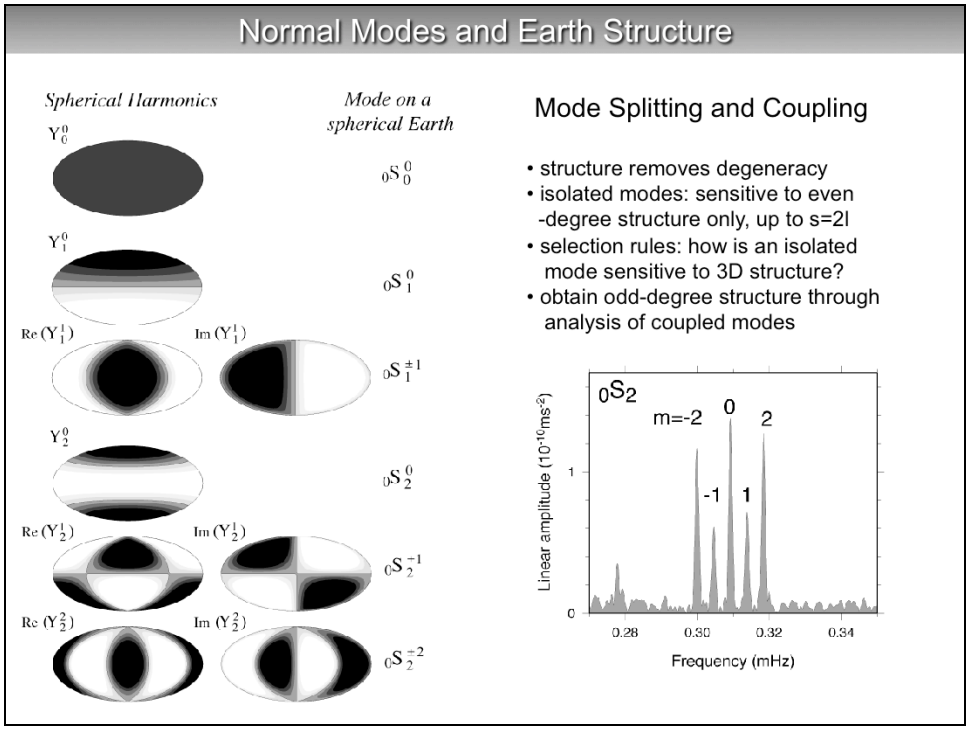

so far, we have treated each of the normal modes as being represented by single spectral peaks; in reality, each mode nTl or nSl actually consists of 2l+1 oscillations. For example, 0S2 has 5 distinct patterns laterally that can be represented by spherical harmonics, Y_l^m where $-l \leq m \leq l$ (see left figure). For a 1-dimensional Earth, all these oscillations (the singlets) have the same frequency, and the oscillations are therefore degenerate, like the electron energy levels of an atom. The collection of all singlets of a mode is called the multiplet. In the presence of a magnetic field, these energy levels split apart (Zeeman effect), so that the degeneracy is removed. Earth structure (incl. rotation and ellipticity of the Earth) removes the degeneracy of the singlet frequencies of a mode in a similar way.

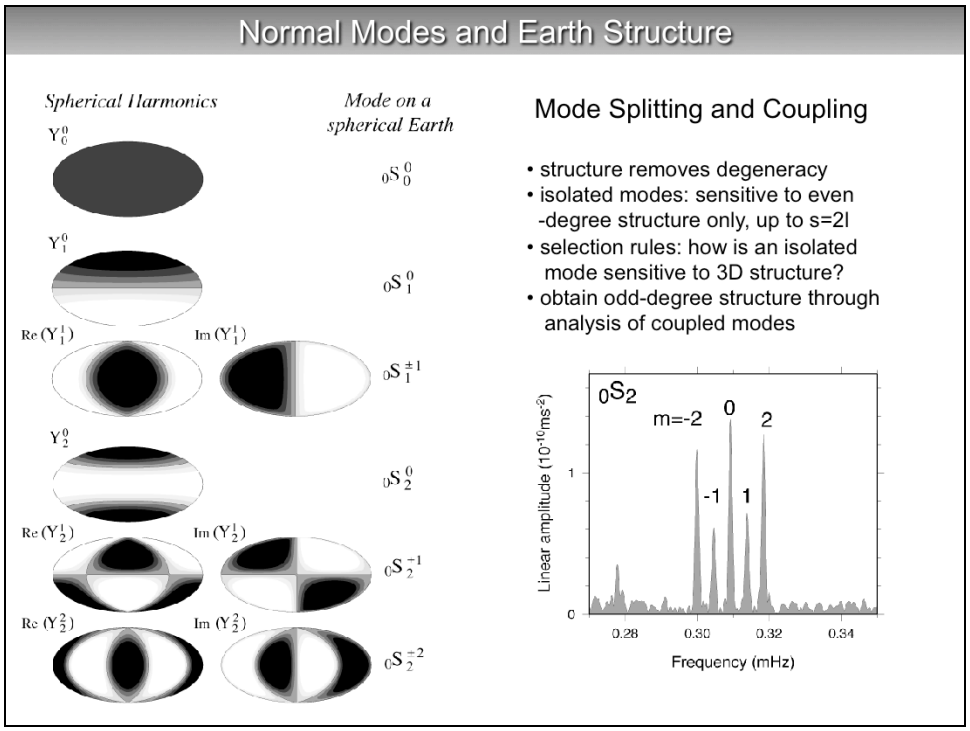

By measuring the frequencies of the split singlets, we can examine Earth structure. The spectrum on the right shows the spectrum of mode 0S2 as observed at a single station. To be able to resolve all singlets in a spectrum, we need very long time series. In practice, this is not possible for most modes because they decay too fast. However, geographical stacking techniques or other analysis techniques that account for overlapping spectral peaks allow us to analyze mode singlets, or in more general terms, the splitting properties of a normal mode.

A normal mode nTl or nSl is sensitive to Earth structure c_s^t up to harmonic degree s=2l. When analyzing each normal mode by itself (treat normal modes as isolated modes), one can determine symmetric structure only, i.e. even-degree structure. So, mode 0S2 helps constrain structure with

s=0,2 and 4. In reality, modes are not isolated but coupled. Coupling is strongest for pairs of modes whose oscillation patterns compare according

to certain rules (the selection rules) and whose frequencies are very close. Though mode-coupling is more difficult to observe, it allows

us to constrain odd-degree structure.

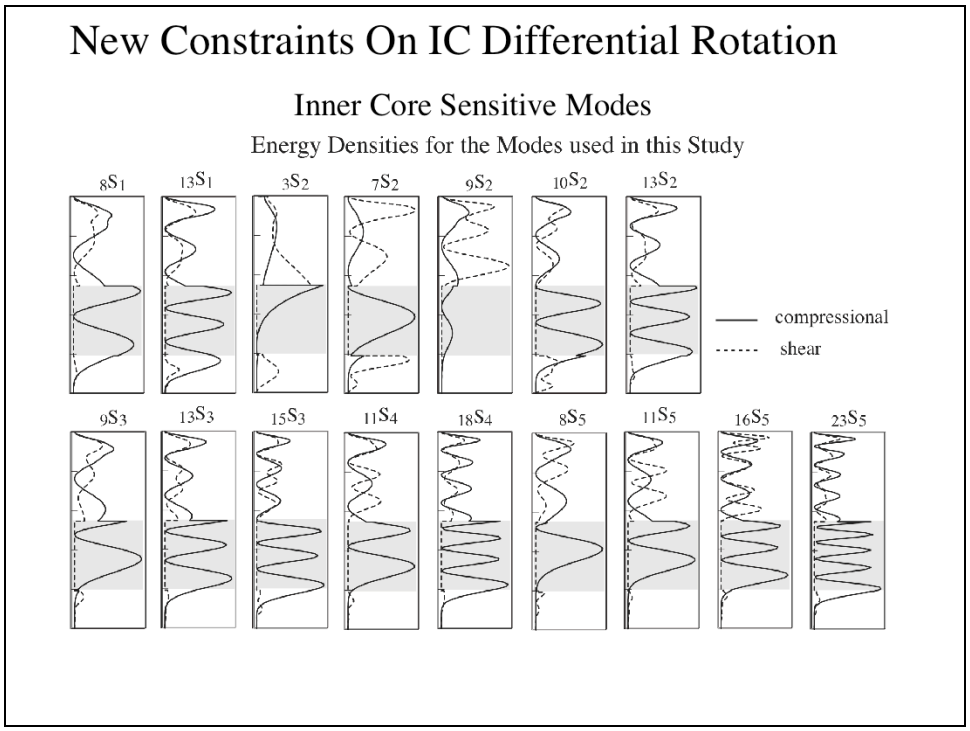

Example 1 of an application of normal modes to investigate Earth.

We examine inner-core sensitive modes to investigate the inner-core differential rotation.

References:

Laske, G. and G. Masters, Limits on differential rotation of the inner core from an analysis of the Earth's free oscillations. Nature, 402, 66-68, 1999.

Laske, G. and Masters, G., The Earth's Free Oscillations and the Differential Rotation of the Inner Core. AGU Geodynamics series, "Earth's Core; Dynamics, Structure, Rotation", Vol. 31, 5-21, 2003.

Song, X., and P.G. Richards (1996), Seismological evidence for differential rotation of the Earth's inner core, Nature, 382, 221-224.

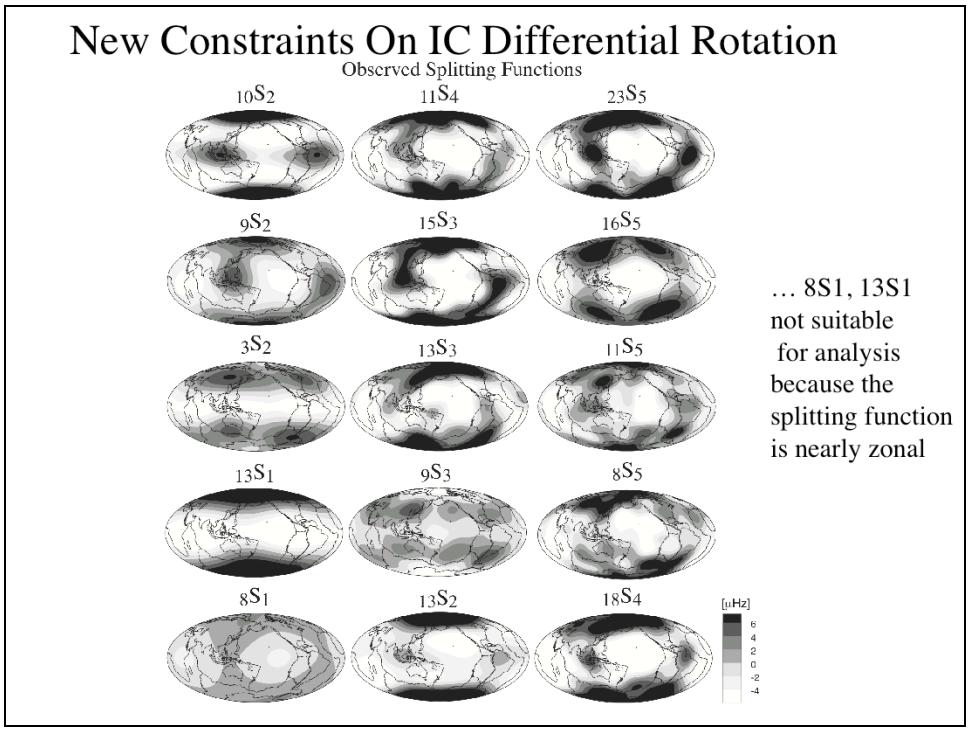

this plot shows splitting functions of inner-core sensitive modes. Splitting functions are similar to surface wave dispersion maps

but show local anomalies in mode frequency anomalies (caused by 3-D structure) instead of local phase or group velocity.

The splitting functions shown here are from or 2003 study. Splitting functions of inner-core sensitive modes are dominated

by zonal structure (depends only on latitude) and they look very different from those of mantle-sensitive modes,

indicating the inner-core structure is mostly symmetric to Earth's rotation axis (see next slide). However, there is a

small amount of non-zonal structure (dependent on longitude) that allows us to examine if the inner core has rotated

over the past few decades.

New Constraints On IC Differential Rotation

Inner Core Sensitive Modes
Mantle and Core Contribution

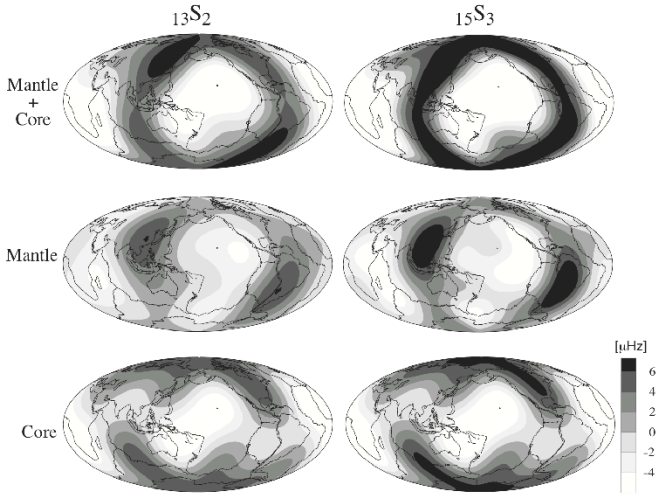

two examples from the 2003 AGU monograph paper to illustrate how different mantle and inner core structure appears in a splitting function. The top panels shows splitting functions that result form mantle and core structure (the observed one). The middle panels show splitting function predictions from an Earth mantle model (as determined by tomographic inversions of body waves and other seismic data), and the bottom panels show splitting functions of the residuals when subtracting the effects from the mantle. In principle, we are left with structure in the outer AND inner core. We assume here that the outer core does not have any heterogeneity so that all signal has to come from the inner core. To examine inner core differential rotation, we now set up a hypothesis test:

1) we determine splitting functions using only recent earthquakes, for all the modes shown in the last slide;
2) for each mode, we subtract the mantle signal;
3) in a forward-modeling approach, we now rotate the core residual signal by an angle, add the mantle back in to make a splitting function for the past and ask which angle is required to best fit the spectral lines for a past earthquakes. For each mode, we then get a rotation angle for each past earthquake;

4) for each mode, a regression line with a rotation rate is then fit to the rotation angles;

5) assuming that the inner core rotates as a rigid body, the rotation rates of all modes have to be the same, i.e. we average over all modes to obtain our best estimate from the differential rotation of the inner core.

New Constraints On IC Differential Rotation

Inner Core Sensitive Modes
Mantle and Core Contribution

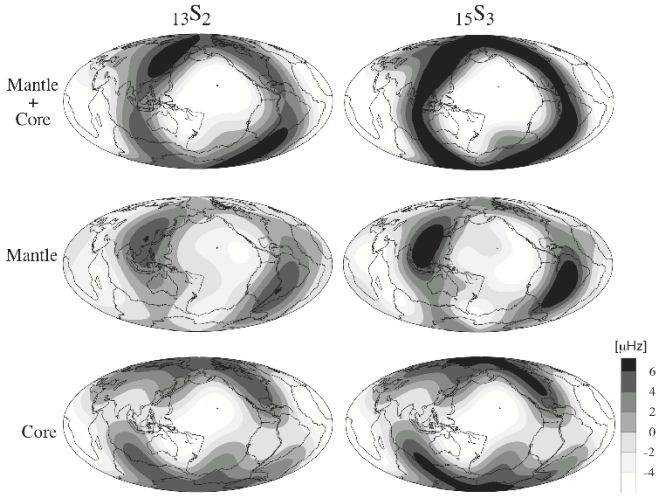

The beauty of analyzing modes for this purpose rather than analyzing individual body-wave waveforms is that we do not have to make any assumptions about what causes the anomalies in the splitting functions (anisotropy or lateral heterogeneity). All we want to examine is if the pattern rotates with time.

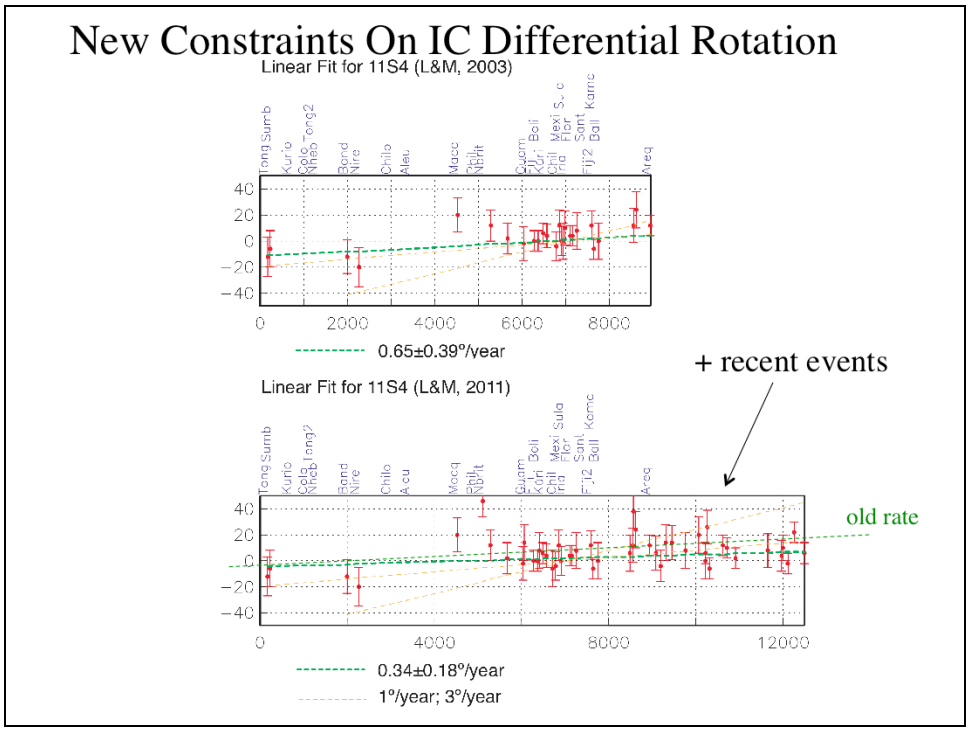

estimation for 11S4 as an example, for our recent 2011 study that include all recent earthquakes. The x-axis in time in days from the oldest earthquake we have (1978 Tonga), the y-axis is the rotation angle in deg. Clearly, a rotation rate of 1 deg/year as initially proposed by others in 1996 is incompatible with our observations. Even smaller rotation rates are not compatible with our data.

New Constraints On IC Differential Rotation

L&M, 2003

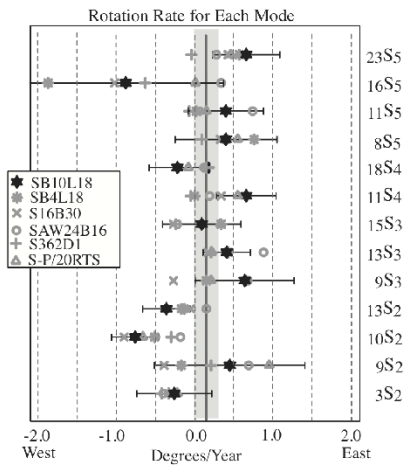

0.13±0.11°/year

L&M, 2011

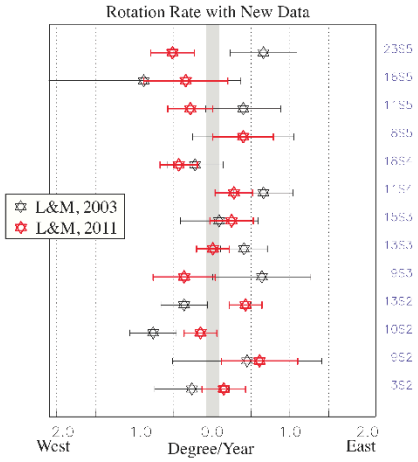

0.00±0.06°/year

best-estimates of rotation rates, for each mode, and the statistical average over all modes, for our 2003 study and the most recent 2011 study. For the L&M (2011) estimation, we use SB10L18 as our preferred mantle model. The 2003 study showed that using different mantle models may give slightly different estimates thought they lie within our error bars. Most recent estimates are now closer to zero resulting in an overall smaller rotation rate where the limit is now reduced by a factor 2 (grey bar).

The bottom line here is that, over the past 35 years, the inner core has had no super-rotation. However, there is some indication that the core may have a changing differential rotation on a decadal time scale.

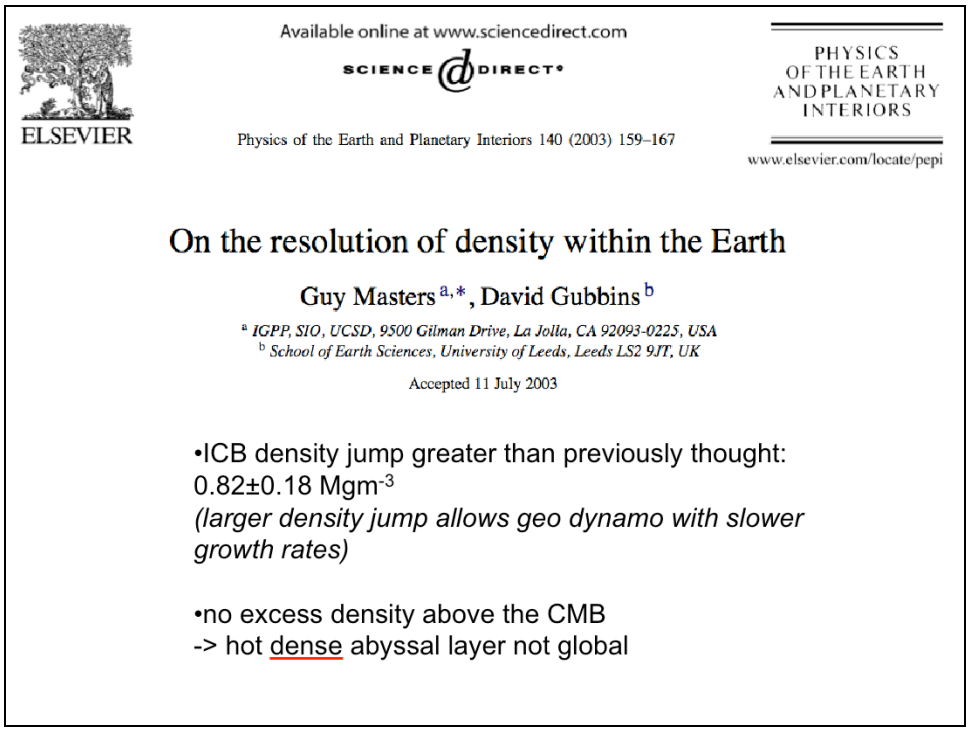

Available online at www.sciencedirect.com
SCIENCE DIRECT®
Physics of the Earth and Planetary Interiors 140 (2003) 159–167
PHYSICS OF THE EARTH AND PLANETARY INTERIORS
www.elsevier.com/locate/pepi

On the resolution of density within the Earth

Guy Masters [a,*], David Gubbins [b]
[a] IGPP, SIO, UCSD, 9500 Gilman Drive, La Jolla, CA 92093-0225, USA
[b] School of Earth Sciences, University of Leeds, Leeds LS2 9JT, UK

Accepted 11 July 2003

•ICB density jump greater than previously thought:
0.82±0.18 Mgm^{-3}
(larger density jump allows geo dynamo with slower growth rates)

•no excess density above the CMB
-> hot dense abyssal layer not global

a second example of a mode study is the use of normal modes to constrain Earth's density. In particular, Masters and Gubbins performed a detailed resolution analysis to obtain a best estimate for the density jump across the inner core boundary. This information is important to constrain the growth rate of the inner core. Another test revolves around the "hot abyssal layer" associated with the two large low-shear velocity provinces in the lowermost mantle beneath Africa and the central Pacific Ocean. An earlier mode study(*) suggested that these anomalies are associated with higher-density material as expected for core-contaminated accumulating material in the region. The test provided new boundaries for the proposed excess density above the CMB:

distributed over 200 km from the CMB (the area over which modes would smear Earth structure at these depths), excess density cannot be larger than 0.4%. This is for the global average, meaning that there is room to accommodate local thin piles of dense material, as long as the global average is not affected beyond the limits given in the last sentence.

(*) **Ishii**, M., & Tromp, J., 1999. Normal-mode and free-air gravity constraints on lateral variations in velocity and density of the Earth's mantle. *Science* **285**, 1231-1236.

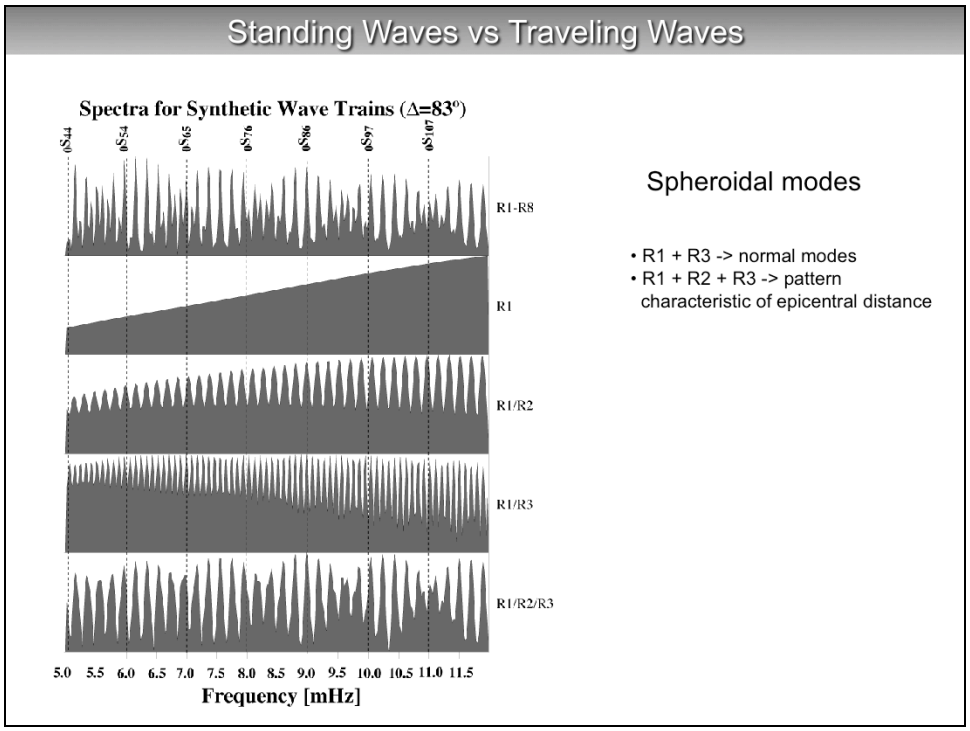

We will now move away from modes. It is interesting to see how standing waves (here, fundamental spheroidal modes) on the Earth form from the interferences/superposition of traveling waves (here, Rayleigh waves).

The top plot shows a spectrum from a 12-h long time series that includes all wave trains from R1 to R8 (the spectrum as we would observe it). The lower panels show spectra when only certain wavetrains are included. A single traveling wave, such as R1, does not know that Earth is a finite body, some the spectrum is continuous. Amplitudes vary with frequency according to the source spectrum and wave dispersion along the travel path. With just one repeat orbit (i.e. R1 + R3), the Rayleigh wave now knows that Earth is finite, and all normal mode peaks form (4^{th} panel from the top).

To obtain the amplitude modulation pattern as seen in the "real" spectrum, that is characteristic of the epicentral distance of the recording station, one needs the addition of one wavetrain traveling in the opposite direction (i.e. R2, lowermost panel).

Standing Waves vs Traveling Waves

Standing waves and travelling waves

- Seismogram as a mode sum:

$$s(t) = \sum_k A_k \cos(\omega_k t + \phi_k) e^{-\alpha_k t}$$

In epicentral coordinates, A_k includes both the source excitations and the geometrical mode behavior as a function of epicentral distance, Δ. This latter term is proportional to a spherical harmonic Y_l^m. For surfaces waves, l is large and m is small then

$$Y_l^m \simeq \frac{1}{\pi\sqrt{\sin\Delta}} \cos\left[(l+\tfrac{1}{2})\Delta - \frac{\pi}{4} + \cancel{\frac{m\pi}{2}}\right] e^{im\phi}$$

Jeans formula is $ka = l + \frac{1}{2}$ so, with arc distance given by $x = a\Delta$

$$Y_l^m \simeq \frac{1}{\pi\sqrt{\sin\Delta}} \cos\left[kx - \frac{\pi}{4} + \cancel{\frac{m\pi}{2}}\right] e^{im\phi}$$

The seismogram of a single mode becomes proportional to a plane wave:

$$s(t) \propto e^{i(\omega t - kx)}$$

$$P_\ell(\cos\Delta) \simeq \left(\frac{2}{\pi\ell\sin\Delta}\right)^{1/2} \cos\left[\left(\ell+\frac{1}{2}\right)\Delta - \frac{\pi}{4}\right]$$

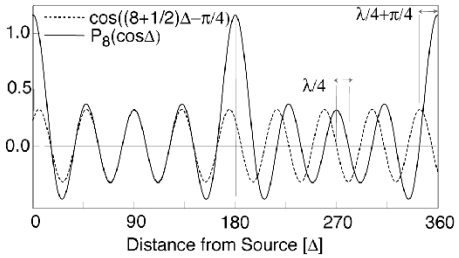

- π/2 phase shift for every polar passage
- (N-1)π/2 phase correction, where N is wave orbit number (e.g. 1 for R1)

a mode seismogram can be considered as the Fourier sum of modes (here represented by cosines) where the amplitude factor, Ak, of a mode with index k depends on a spherical harmonic Y_l^m, where the Y_l^m is proportional to a Legendre polynomial P_l (top right).

For surface waves, l is large and m is small so that the Y_l^m can be approximated by cosines. This works well at places away from the earthquake and away from the antipode (the poles). But whenever a surface wave passes a pole, there is a phase shift of pi/2 (a lag) which needs to be added back in. So, for a wave train RN, the phase correction is (N-1)pi/2, i.e. R1 has no correction because it has not yet passed a pole.

Phase and Group Velocity

Phase and group velocity

In general $k = k(\omega)$ (dispersion). The mode sum can be written as an integral over frequency:

$$s(x,t) = \int B(\omega) e^{i(\omega t - k(\omega)x)}\, d\omega$$

$B(\omega$ is due to the source – slowly varying. Consider f, the phase:

$$f = \omega t - k(\omega)x$$

The main contribution to the integral is when phase is stationary ($df/d\omega = 0$). If ω_s is the point where the phase is stationary, we have

$$t - \frac{dk}{d\omega}(\omega_s)x = 0$$

Define the group velocity, U:

$$U = \frac{x}{t} = \frac{d\omega}{dk}$$

The energy associated with a particular frequency group centered on ω_s travels with the group velocity $U(\omega_s)$

traveling waves contribute most to a seismogram when the phase is stationary with respect to time and frequency. So, e.g. the frequency-derivative of the phase with respect to omega (or k of omega, where k is the wavenumber) has to be zero. From that one obtains the

condition for the group velocity, u=x/t=domega/dk. The phase velocity is, c=omega/k.

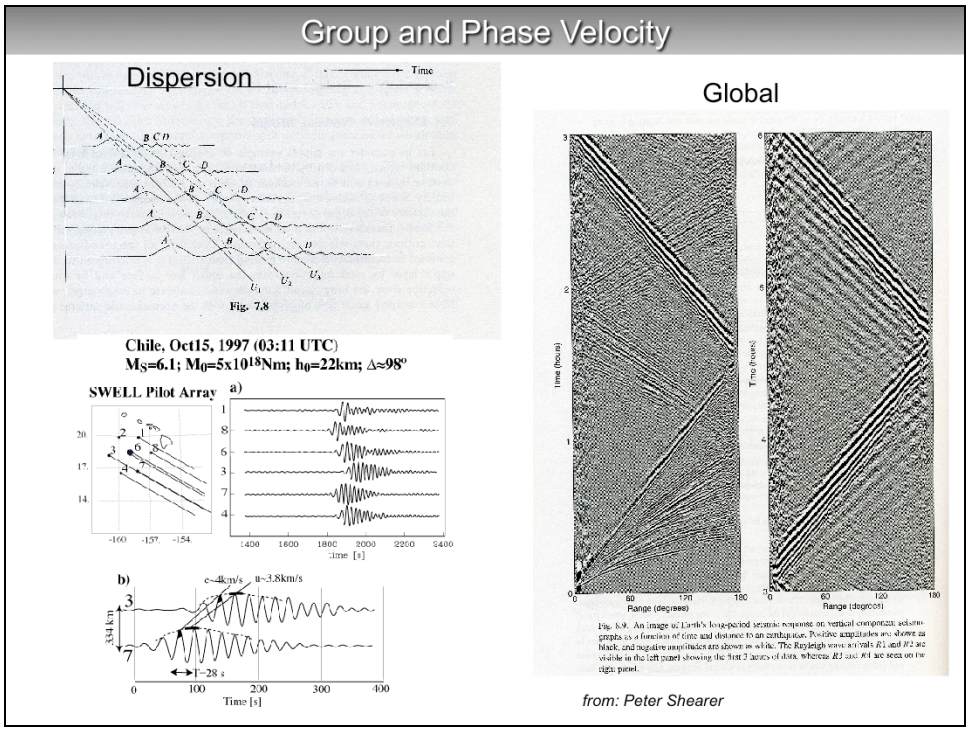

for a dispersed wavetrain, group and phase velocity are different and depend on frequency. Dispersion also implies that, over time or over distance traveled, a wavetrain gets pulled apart (upper left panel). The right panels shows, as function of travel distance, how R1 is more compact in

time but R2, R3 and R4, which traveled over a greater distance, are successively wider in time. We obtain the group velocity of a narrow-frequency-band wave packet by measuring the traveltime of the maximum of the envelope (left lowermost panel). The group velocity is a measure of energy transport.

A particular phase within the wave packet travels with the phase velocity.

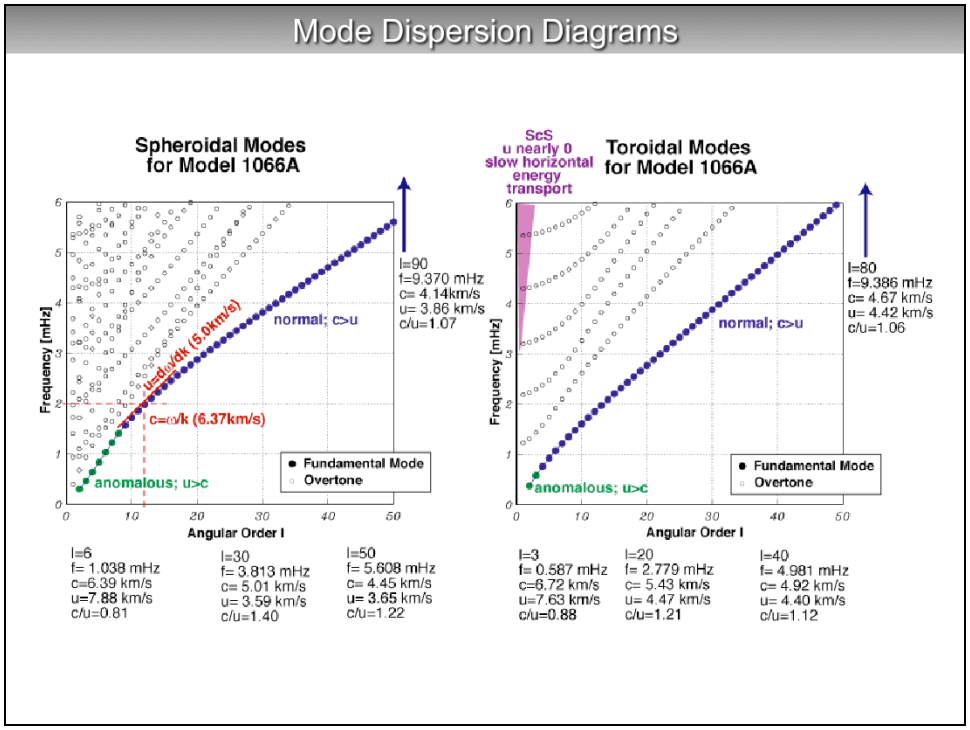

getting back to the mode dispersion diagram, we can now examine the behavior of group velocity, domega/dk or domega/dl (k=(l+1/2)/a;

a=earth radius), and phase velocity omega/k. The fundamental modes (Love and Rayleigh waves) are color-coded. For most long-period

surface waves up to 6 mHz (or modes up to l=50),

c>u and dispersion is normal. For some low-l modes, c<u and dispersion is anomalous.

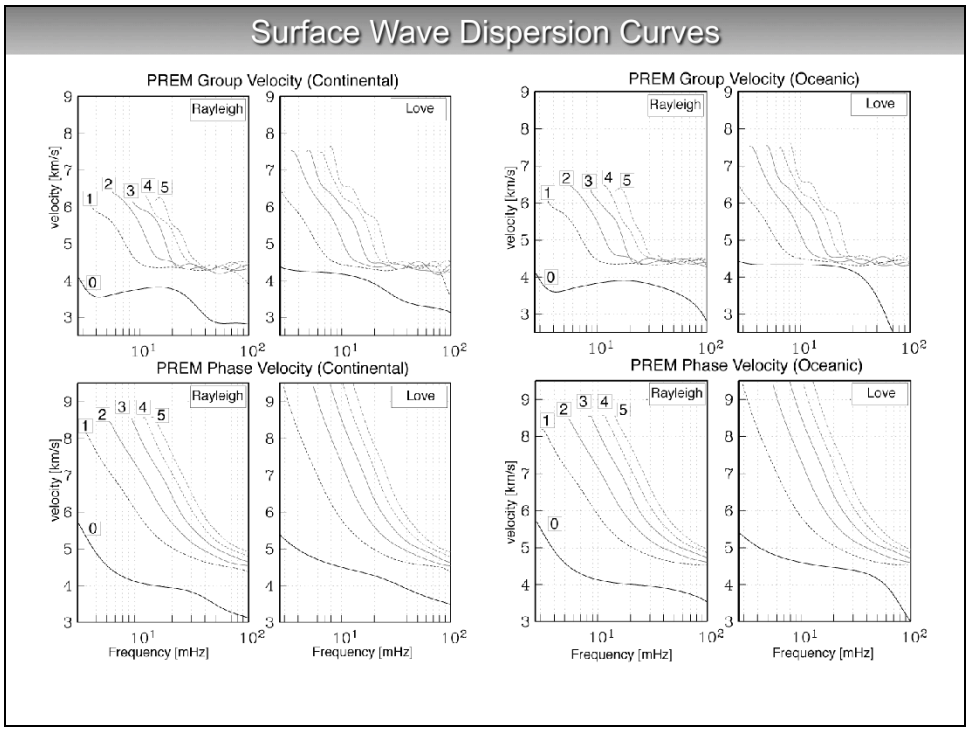

the diagrams here show dispersion from a traveling wave point of view. We show dispersion curves for two types or Earth structure: continents (left group of 8 panels) and oceans (right group); in each of the two, we show group (top two) and phase velocity (bottom two); Rayleigh waves (left two) and Love waves (right two). Shown are dispersion curves for fundamental modes (0) as well as the first 5 overtones.

In general, phase velocity is larger than group velocity, Love wave velocities are larger than Rayleigh wave velocities, except at higher frequencies for oceans, when Love wave velocities drop rather sharply. The fundamental mode is usually isolated and it is easy to measure phase and group velocity, except for purely oceanic paths where group velocities of the fundamental mode overlap with those of the overtones. This means that fundamental modes and overtones arrive at the station at the same time so that measurement of either group or phase velocity is not possible, or at the very least, velocity estimated for the fundamental mode may be biased by overtone contamination.

A trick that helps in this case is to use only earthquakes with shallow source depths because shallow earthquakes usually excite fundamental modes more strongly relative to overtones than deeper earthquakes do. For fundamental mode surface wave studies, we usually use only earthquakes with source depths less than 200 km.

It is much more difficult to separate the different overtone branches as their group velocities overlap even more. in regional studies, an array of seismometers helps to perform omega-k analyses to separate the different overtone branches.

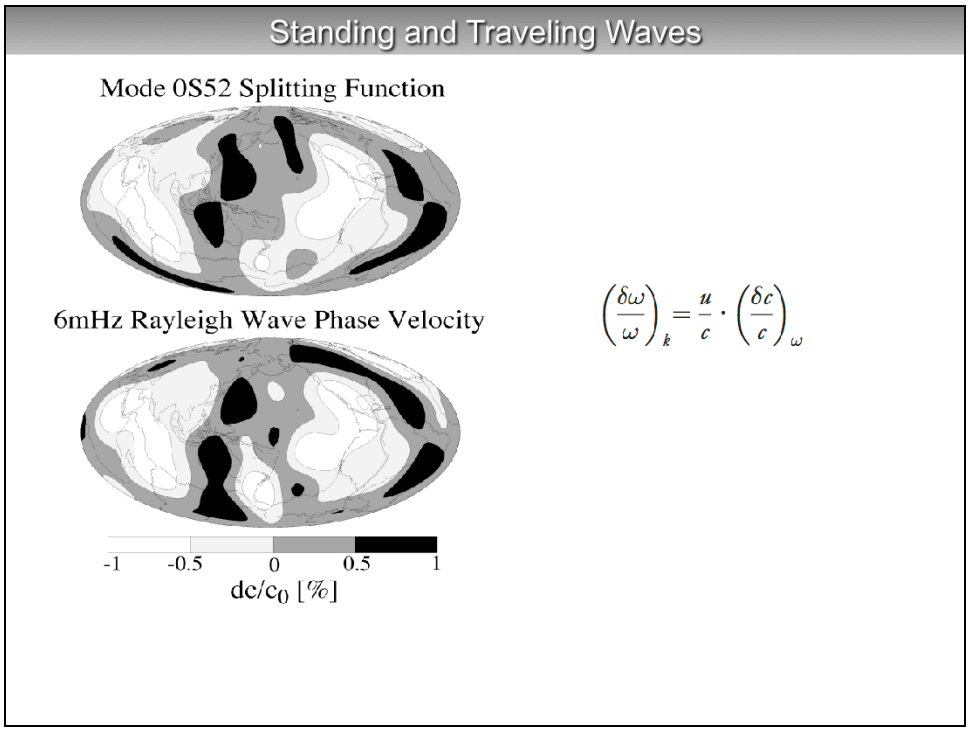

assuming we have measured local mode frequency anomalies (splitting function) in the standing-wave regime and local phase velocity anomaly in the traveling wave regime, we can verify that both wave regimes image Earth structure in the same way. We have to remember though that isolated modes are sensitive to even-degree structure only, so we have to remove the odd-harmonic degrees in a phase velocity map. There also exists a scaling factor, u/c, between mode frequency anomalies and phase velocity anomalies.

Taking these into account, the splitting function of a Spheroidal mode and the Rayleigh wave phase velocity map at the corresponding frequency are extremely similar even though these maps were obtained using completely different data and measurement techniques. This close resemblance underlines the quality of both datasets.

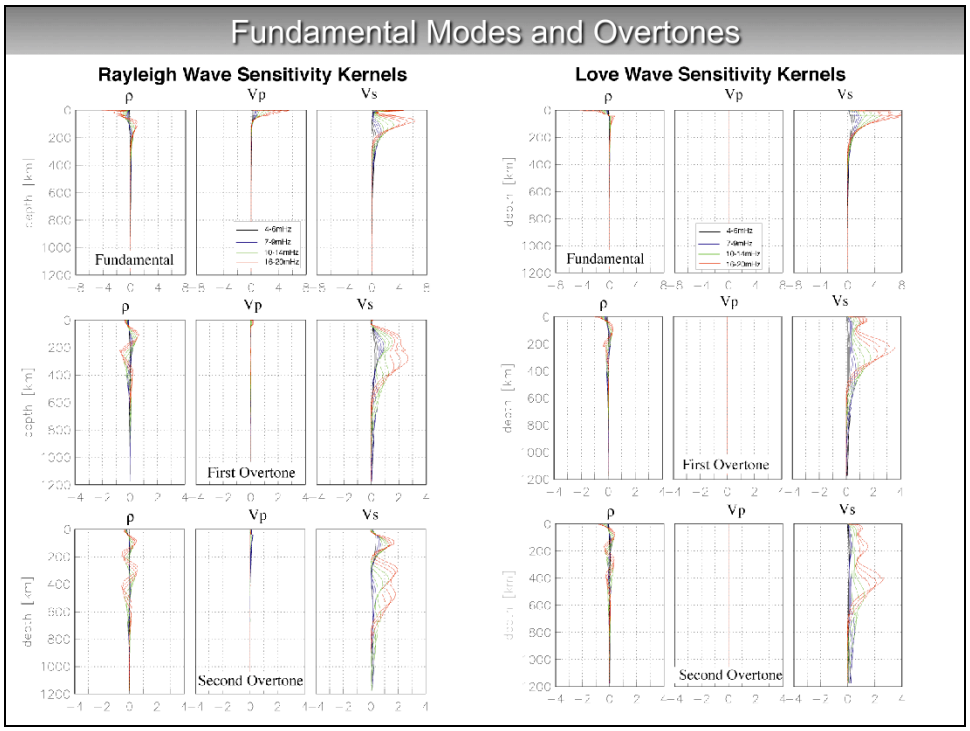

after we have determined dispersion as function of frequency, we can then obtain structural models with depth.

Several things are important to realize:

1) Rayleigh waves are strongly sensitive to Vs but there us also sensitivity to density as well as shallow Vp.

2) Love waves are sensitive to Vs and density only.

3) Love wave kernels are much more similar as frequency varies

so the resolution for Vs with depth is less than with Rayleigh waves (there are effectively less orthogonal eigenvectors).

4) Adding overtones in the modeling helps resolve deeper structure.

Transverse Isotropy

- also known as radial anisotropy (or polarization anisotropy)
- as result of incompatibility of Love and Rayleigh wave dispersion
- usually independent Love/Rayl inversions
- but: Love sensitive to V_{SV}!

$$A = \rho V_{PH}^2 = \tfrac{3}{8}(C_{11} + C_{22}) + \tfrac{1}{2}C_{12} + \tfrac{1}{2}C_{66}$$

$$C = \rho V_{PV}^2 = C_{33}$$

$$L = \rho V_{SV}^2 = \tfrac{1}{2}(C_{44} + C_{55})$$

$$N = \rho V_{SH}^2 = \tfrac{1}{8}(C_{11} + C_{22}) - \tfrac{1}{4}C_{12} - \tfrac{1}{2}C_{66}$$

$$F = \tfrac{1}{2}(C_{13} + C_{23})$$

$$\eta = F/(A - 2L)$$

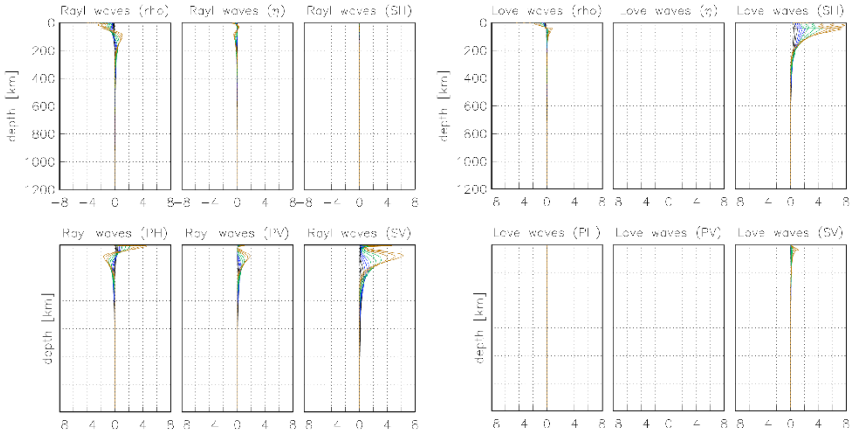

at least in the upper mantle, Earth is transversely isotropic, i.e. horizontal velocities are different from vertical velocities;

here, Rayleigh waves are still only sensitive to Vsv and Love waves are primarily sensitive to Vsh but Love waves now also have a weak sensitivity to Vsv though this is usually ignored to keep the number of model parameters small (but, strictly speaking, one would have to invert for Vsh(z), density(z) and Vsv(z); z= depth). Also note that Rayleigh waves are sensitive to both Vpv and Vph.

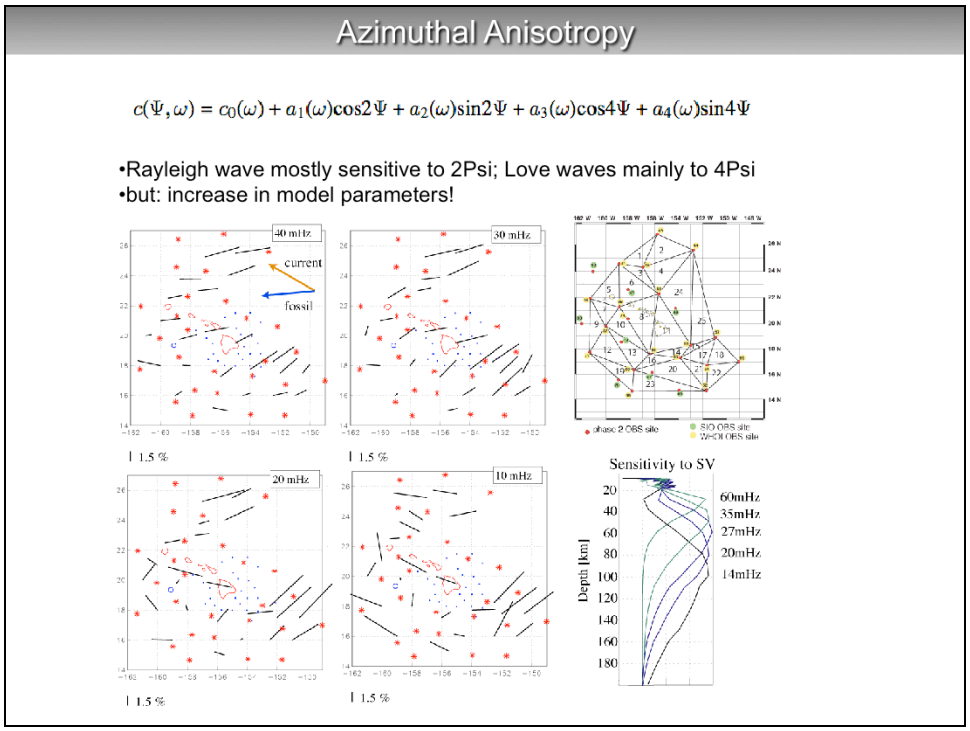

in addition to transverse isotropy, non-vertical mantle flow, mineral texture and strain causes azimuthal anisotropy that in turn causes seismic shear-wave splitting and surface wave azimuthal anisotropy. For weak anisotropy, the phase velocity, as function of azimuth, psi, is expressed as a truncated trigonometric series (Smith and Dahlen, 1973, based on the more general formulation by Backus, 1965). For realistic anisotropic mineralogies, the 4-psi terms can usually be ignored for Rayleigh waves and the 2-psi terms for Love waves. The example here shows Rayeligh fast directions (2-psi terms)

and the strength of azimuthal anisoptropy observed during a temporary ocean-bottom-seismometer deployment around Hawaii. For higher frequencies, the fast directions align roughly with the fossil spreading direction (i.e. “frozen” into the lower lithosphere), while the pattern at lower frequencies (that sample into the asthenosphere) are indicative of a mantle flow along the present spreading direction that is perturbed (by a mantle plume?) near Hawaii.

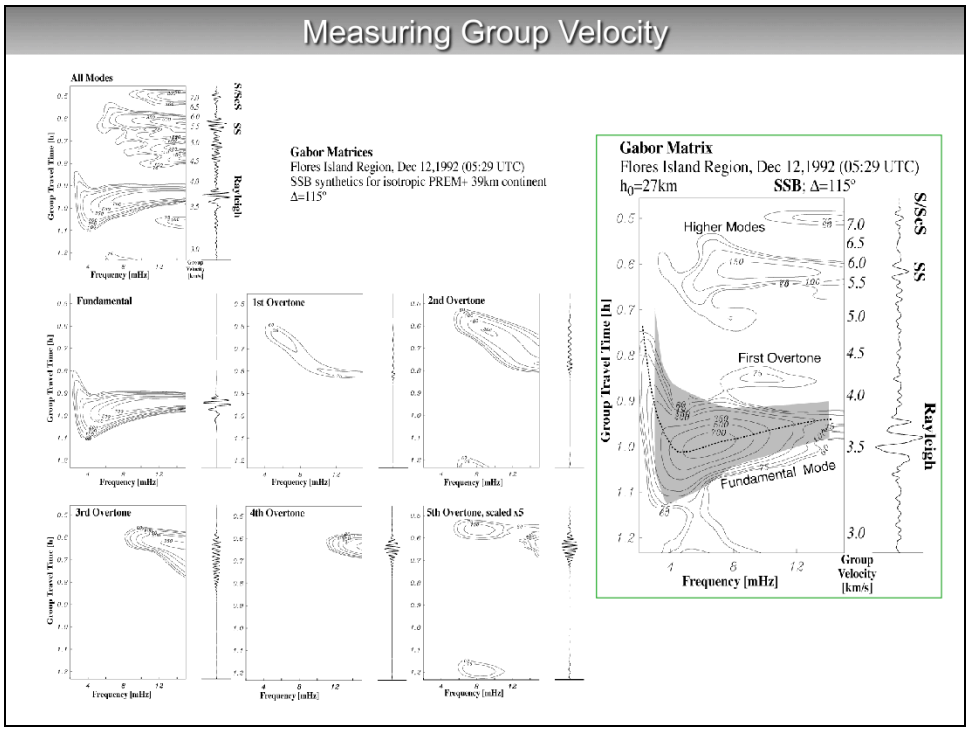

without going into much detail, the next few slides describe some points that need to be considered when measuring dispersion. The panels shown here are time-frequency plots which help determine group velocities (pioneered by Adam Dziewonski and colleagues in the 1960s). In essence, we choose a small time window, determine the amplitude spectrum and tabulate it as a line in a matrix. The next line in the matrix is composed by a spectrum calculated for a slightly later time window …. and so on … until we have a matrix showing the frequency-dependent (x-axis) amplitudes as function of time (y-axis, starting at the top!) (note that squared amplitudes are proportional to energy). The group velocity is then easily determined by picking

the maxima along the amplitude ridges.

The left panels here show how the different overtone branches contribute to the seismogram. This is the principle of measuring group velocity. In practice, we measure group velocity with respect to either a synthetic seismogram or another seismogram recorded along the source-receiver great circle (two-station method). This reduces dispersion and allows for more accurate measurements as function of frequency.

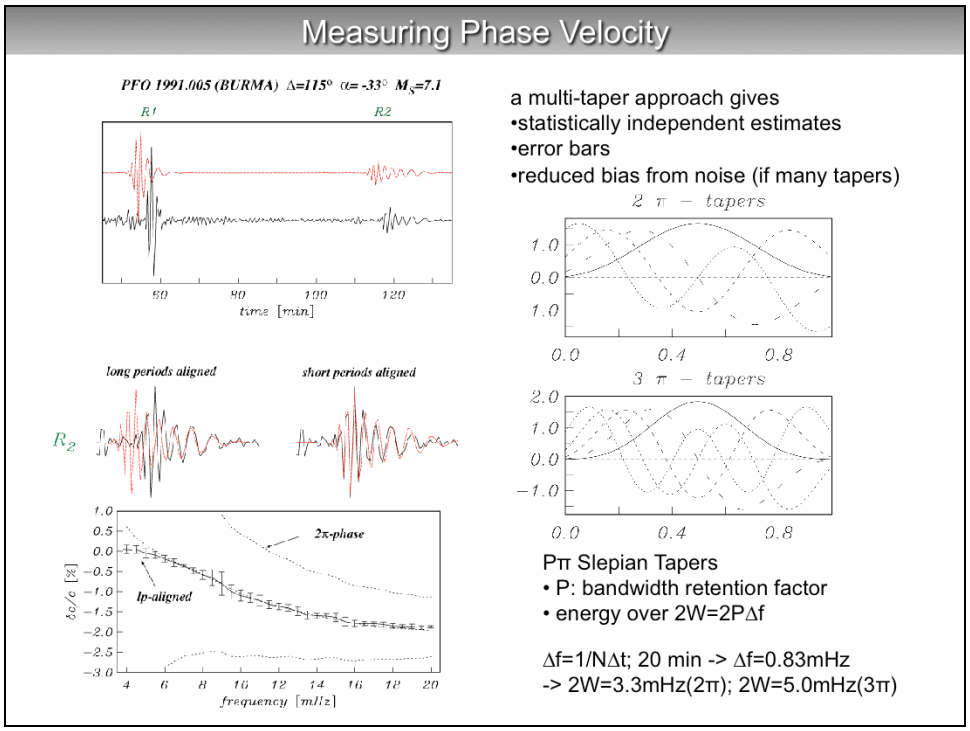

as mentioned previously, phase velocities are determined by the propagation of the actual wiggle within a wavepacket. As with group travel time, the phase changes quickly with frequency (see next slide). Since the wave packets are compact in time (15 min or so), short time windows do not allow for very fine frequency sampling and spectral estimates are strongly smoothed over a relatively wide frequency range (see bottom on the right). To obtain precise phase estimates, we therefore measure phase with respect to a synthetic or the seismogram of a second station (e.g. in the two-station method).

To further reduce the rapid change of phase with frequency (which is relevant for the measuring process only!) we try to align the two seismograms (since a time shift corresponds to a known linear increase of the phase with frequency, this can later be added back to the measured phase very easily!!). The alignment does not have to be perfect. All we want is to reduce the rapid change with frequency as much as possible to allow the retrieval of the phase measurement as precisely as possible.

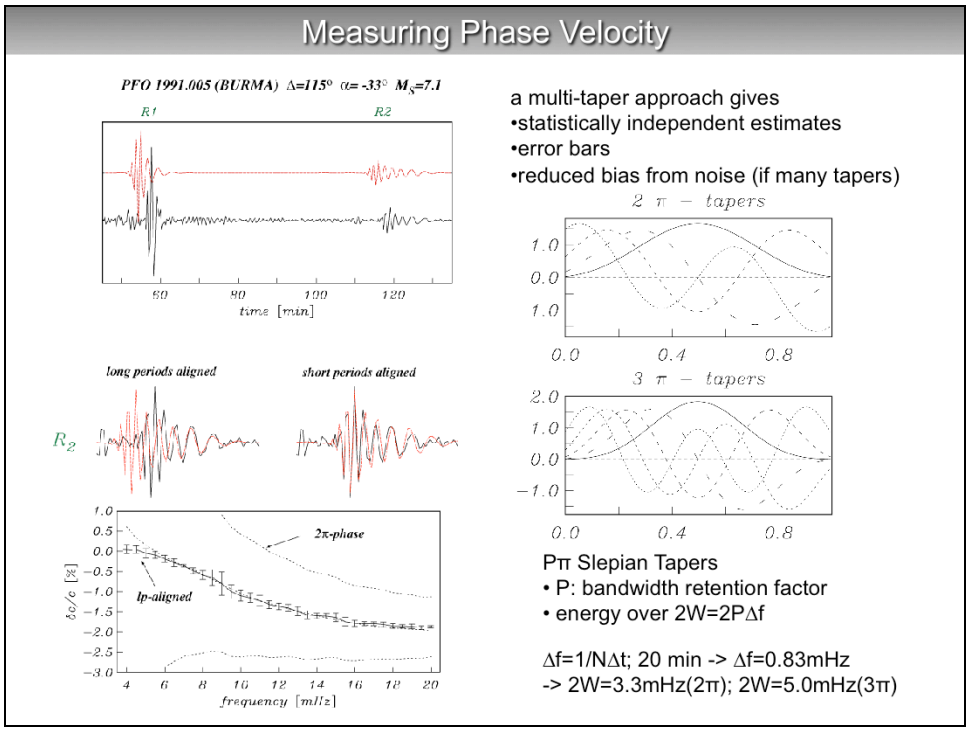

Unlike with group travel time, we have to worry about the 2pi phase ambiguity as we measure phase only between –pi and pi. As illustrated on the lowermost left panel, it is relatively easy to determine the "right amount" of n2pi in the phase at low-frequency as adding or subtracting 2pi would lead to unrealistic phase velocities. But this is not so at higher frequencies. We therefore start at low frequencies and then require that the phase be continuous as function of frequency. This requirement allows us to add the right amount of npi to the phase. We also use a multi-taper approach instead of a single-taper approach that uses a boxcar or Hanning tapers. The Slepian prolate spheroidal Ppi eigenfunction tapers are orthogonal so spectral estimates using these tapers give statistically independent estimates, which allows us to assign measurement errors. The multi-taper approach also optimizes between bias from contamination by incoherent noise and spectral smearing effects.

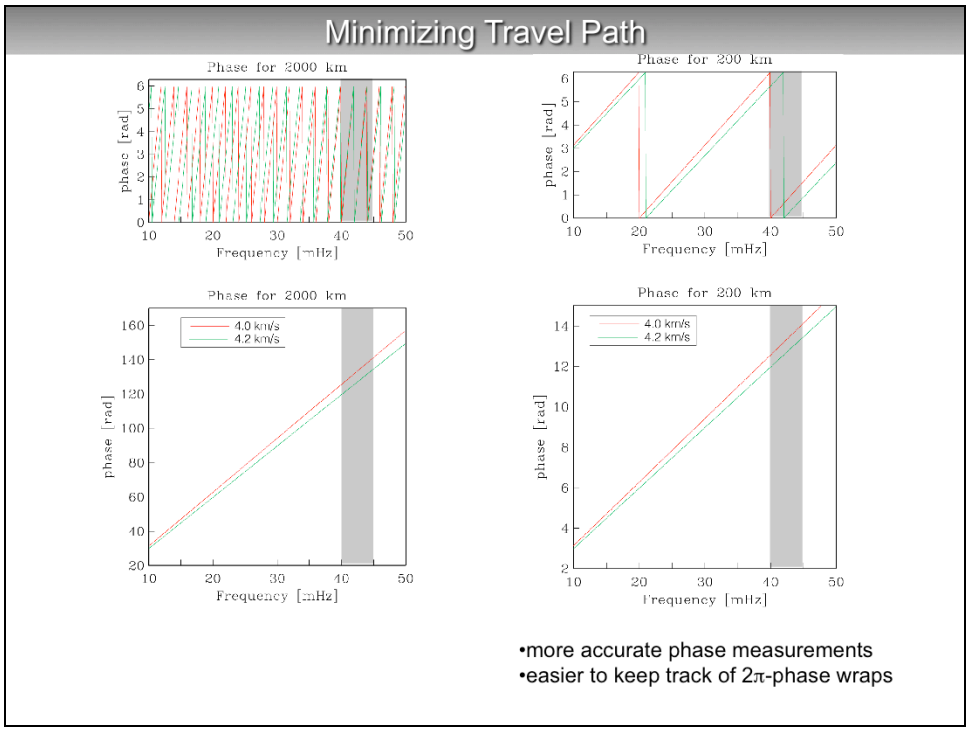

these panels show two cases of how quickly the phase really changes with frequency, for a distance of 2000 km (left) and 200 km). The grey bar is 5-mHz frequency range over which a typical phase estimate is smoothed as a result of the finiteness of the time window for analysis (given by the shortness of the wave packet). The upper panels show the phase within a 2pi range, while the lower panels show the unwrapped phase. The point here is that for a travel path of 2000 km, it is nearly impossible to keep track of the 2-pi phase wraps. Even in the case of the 200-km distance, we would try to align the seismogram to remove the linear increase in the phase as much as possible (recall that a lag in the time domain translates to a linear phase increase in the frequency domain).

Measuring Phase Velocity

Measuring Phase

The phase of the Fourier transformed seismogram is just kx (with a source term) but we need to be careful how we measure this to avoid bias. Measure relative phase between data and synthetic of measure phase difference between orbits.
Transfer function approach – single spectral estimate:

$$S_{obs}(\omega) = T(\omega) S_{syn}(\omega)$$

$$T(\omega) = \frac{S_s^*(\omega) S_o(\omega)}{S_s^*(\omega) S_s(\omega)} = \frac{C_{12}(\omega)}{C_{11}(\omega)}$$

Better to use a multi-taper estimate. Minimize

$$\|\mathbf{S}_o(\omega) - T \cdot \mathbf{S}_s(\omega)\|^2$$

$\mathbf{S}_o$ and $\mathbf{S}_s$ are vectors whose components are the spectral estimates at fixed frequency using one of the prolate tapers. The least-squares estimate of the transfer function then is

$$T(\omega) = \frac{\mathbf{S}_o(\omega) \cdot \mathbf{S}_s^*(\omega)}{\mathbf{S}_s(\omega) \cdot \mathbf{S}_s^*(\omega)}.$$

$$T(\omega) = e^{-\delta\gamma(\omega)x} e^{-i\delta k(\omega)x}$$

the measurement of the phase with respect to a reference seismogram can be understood as determining the transfer function between the two seismograms, which is equivalent to a deconvolution in the time domain or the division of spectra in the frequency domain. We prefer to work in the frequency domain.

Measuring Phase Velocity

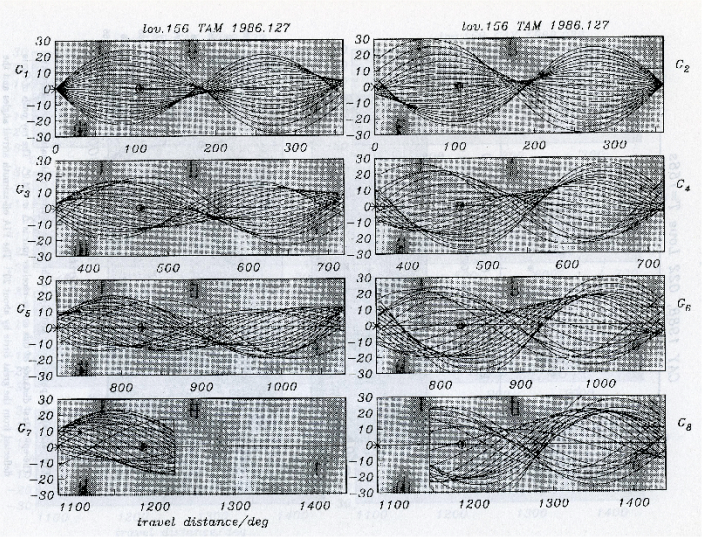

- stay away from caustics
- -> epicentral distance for analysis: $20^\circ \leq \xi \leq 160^\circ$

these panels show the progression of surface waves across Earth's surface where the source-receiver great circle is rotated to lie in the equator (the source is on the left for ode wave orbit numbers, and on the right for even wave orbit numbers). Shown are rays (which are normal to the propagating wave front). Near the source and the antipode, rays come together implying the presence of a caustic. In this case, we cannot measure the phase. The caustics widen for increasing wave orbit numbers.

Measuring Phase Velocity

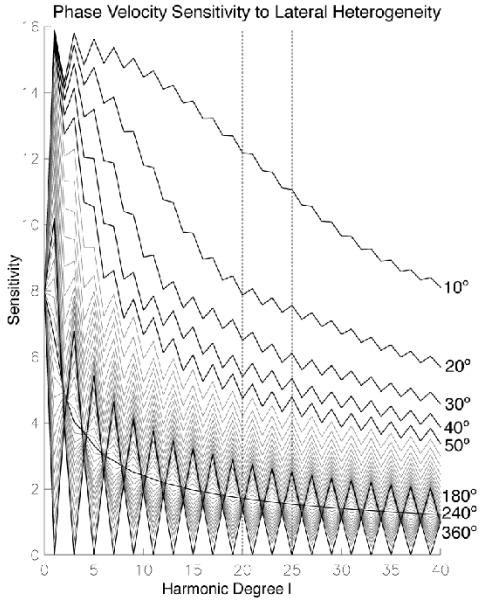

A phase perturbation $\delta\Psi(\omega)/\Psi(\omega)$, caused by lateral heterogeneity, is then

$$\frac{\delta\Psi(\omega)}{\Psi(\omega)} = -\frac{1}{\Delta}\int_0^{\Delta}\frac{\delta c(\omega)}{c_0(\omega)}\,dx \qquad [20]$$

where $\Psi(\omega)$ is the frequency-dependent phase accumulated along the perturbed travel path, Δ is the travel distance, and $c_0(\omega)$ is the frequency-dependent reference phase velocity. Equation [20] is correct to first order in lateral heterogeneity. Pollitz (1994)

On a sphere, it is convenient to expand lateral heterogeneity in terms of surface spherical harmonics $Y_l^m(\theta, \phi)$ as function of geographic coordinates θ and ϕ, so that $\delta c/c_0$ is

$$\frac{\delta c(\omega)}{c_0(\omega)} = \sum_{l=0}^{L_M}\sum_{m=-l}^{l} c_l^m(\omega)\, Y_l^m(\theta,\ \phi) \qquad [21]$$

it is interesting to examine how a phase measurement is sensitive to structure of different wavelength along the travel path. If we expand structure in spherical harmonics, the sensitivity decreases with increasing wavenumber (decreasing wavelength). R1 is more sensitive to odd-degree structure than even-degree structure and the disparity of sensitivity is increasing with distance. The travel path of R2 corresponding to an epicentral distance of 120 deg is 240 deg long. In this case, sensitivity to structure is smooth (i.e. same sensitivity to even and odd degrees). For shorter R2 paths (greater epicentral distance), sensitivity to odd degrees (over even degrees increases). For longer R2 paths (short epicentral distance) sensitivity to even-degree structure increases over that to odd-degree structure. In the extreme case of a complete great-circle path, a Rayleigh wave completely lost sensitivity

to odd-degree structure (equivalent to isolated normal modes).

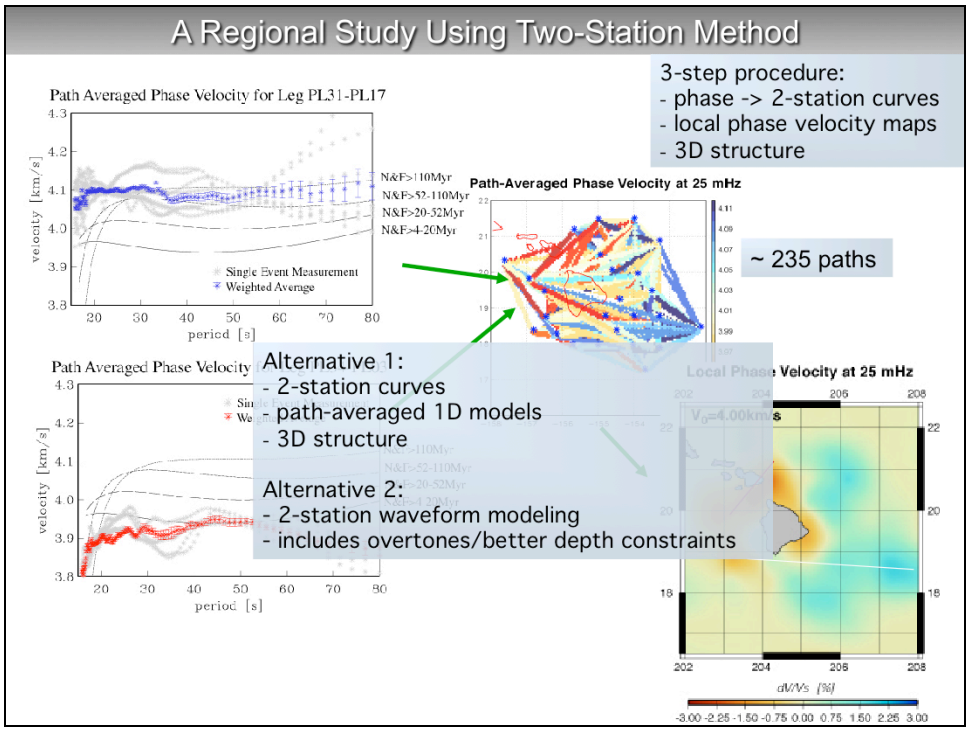

there are different ways to observe dispersion and use it to infer Earth structure. The approaches shown here are for a regional study but this also applies to global studies:

approach 1: as described in previous slides presupposes that the phase was measured (i.e. between a real seismogram and a synthetic globally or between two real seismograms in a regional study); collect dispersion along many paths; these dispersion curves are called “path-averaged”

dispersion curves because they describe the average dispersion between two stations; to obtain actual phase velocities at a location, we input all dispersion curves in an inversion for phase velocity maps, at fixed frequency; the final step then is to use these maps in another inversion for structure at depth (e.g. local Vs(z));

Laske, G., Markee, A., Orcutt, J.A. Wolfe, C.J., Collins, J.A., Solomon, S.C., Detrick, R.S., , Bercovici, D. and Hauri, E.H., Asymmetric Shallow Mantle Structure beneath the Hawaiian Swell - Evidence from Rayleigh Waves Recorded by the PLUME network. Geophys. J. Int., 187, 1725–1742, 2011

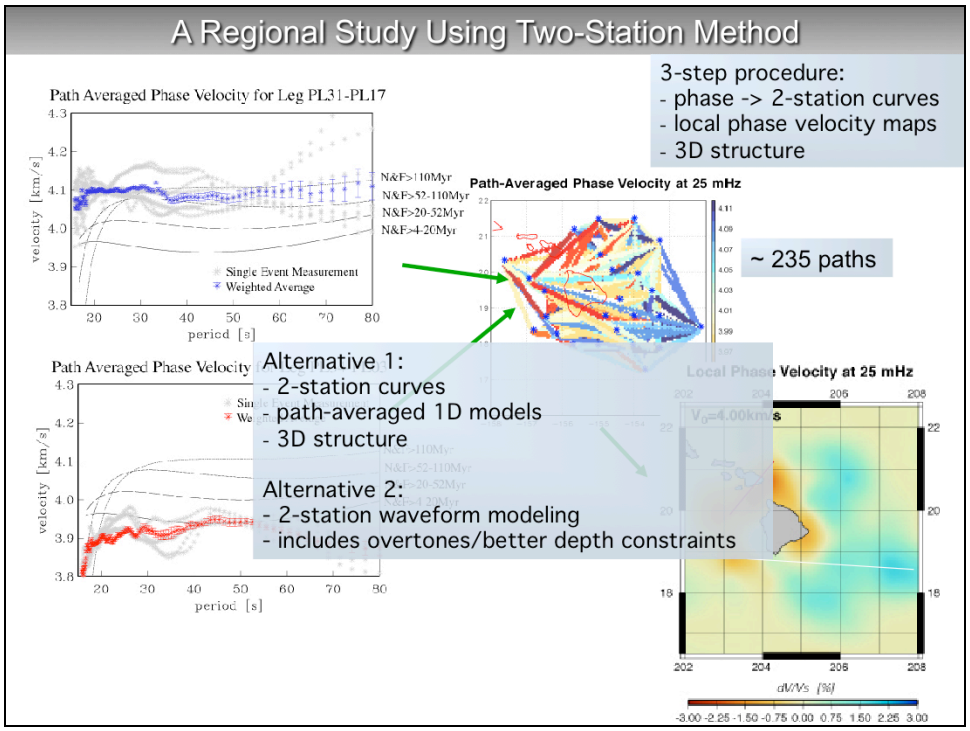

approach 2: here, we take each path-averaged dispersion curve in individual inversions for path-averaged Vs(z); all of the path-averaged Vs(z) are then input in another inversion for local variations in Vs(z), in a map;

approach 3: instead of measuring phase, one can forward-model the actual waveform by changing the underlying Vs(z) and calculating a synthetic seismogram until the synthetic matches the observed seismogram to obtain a path-averaged Vs(z); like in approach 2, these are then used in an inversion for 3-D structure; an advantage of this technique is that overtones (that improve sensitivity to deeper structure) are implicitly included in the modeling; a disadvantage is that it is more difficult to assign error bars to the data and the resulting model; waveform modeling can include mode coupling (another advantage)

Correction for Off-Great Circle Approach

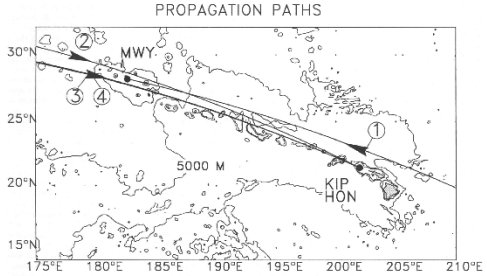

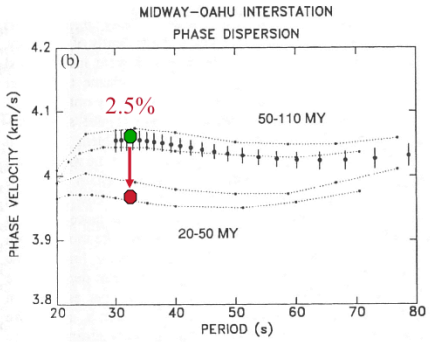

Off-Great Circle Approach

$\Theta = 10^{o} \rightarrow \delta c/c = 1.5\%$
$\Theta = 15^{o} \rightarrow \delta c/c = 3.5\%$
$\Theta = 20^{o} \rightarrow \delta c/c = 6.4\%$

in regional studies using the two-station approach, it is important to account for off-great circle propagation, i.e. if the earthquake does not perfectly lie on the great circle shared by the two stations. To illustrate this point, the table shows the bias in estimated phase velocity when off-great circle approach is not accounted for (using simple trigonometry).

A 2.5% error in the phase measurement would not allow us to distinguish between the seismic signal of 50 and 100 Myr old oceanic lithosphere.

Alternative 3: Helmholtz Tomography

- joint inversion for structure and wavefield, for each earthquake
- need dense network!

from: Lin and Ritzwoller

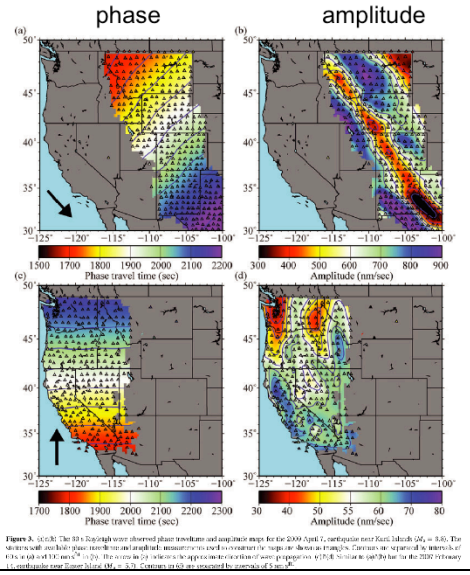

apparent c' from eikonal eq

$$\frac{\hat{k}_i(\mathbf{r})}{c_i'} \cong \nabla\tau_i(\mathbf{r}),$$

structural c from Helmholtz eq

$$\frac{1}{c_i(\mathbf{r})^2} = |\nabla\tau_i(\mathbf{r})|^2 - \frac{\nabla^2 A_i(\mathbf{r})}{A_i(\mathbf{r})\omega^2}$$

important when signal wavelength close to structural wavelength

a technique that was proposed in the early 1990s and found recent application is solving the Helmholtz equation rather than the eikonal equation to obtain phase velocities. Wielandt showed that when the wavelength of a wave reaches the limit of the wavelength of the structure, the passage of a wavefront through a structure is deformed in such a way that the phase velocity measured from the phase along (dynamic phase velocity) is no longer the true phase velocity associated with the structure (structural phase velocity) that we really seek. In this case, the structural phase velocity can be retrieved by measuring the amplitude of the wavefield and correct the dynamic phase velocity. This process requires a dense seismic network, such as the USArray. Shown are examples of the propagating wavefield for two earthquakes (black arrow).

Lin, F.C. and M.H. Ritzwoller, Helmholtz surface wave tomography for isotropic and azimuthally anisotropic structure, Geophys. J. Int., 186, 1104-1120, doi:10.1111/j.1365-246X.2011.05070.x, 2011.

Alternative 3: Helmholtz Tomography

apparent c A correction corrected c *from: Lin and Ritzwoller*

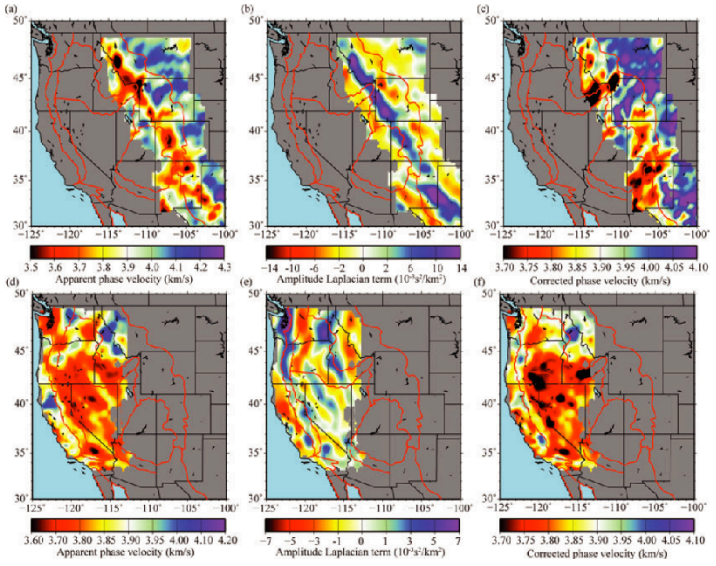

Figure 4. (a) The apparent phase velocity map derived from Fig. 3(a) based on eq. (1). (b) The amplitude correction term in eq. (2) derived from Fig. 3(b). (c) The corrected phase velocity map derived from (a) and (b) based on eq. (2). Same as (a)-(c) but for results derived from Fig. 3(c) and (d).

these panels show apparent (dynamic) phase velocity and corrected phase velocity, for the two earthquakes shown in the last slide.

Attenuation

from: Colleen Dalton

•Rayleigh wave attenuation sensitivity to attenuation at depth

$$Q^{-1}(\omega,\theta,\phi) = \int_0^a \left[\kappa_0(r)K_\kappa(\omega,r)Q_\kappa^{-1}(r,\theta,\phi) + \mu_0(r)K_\mu(\omega,r)Q_\mu^{-1}(r,\theta,\phi)\right] r^2 dr.$$

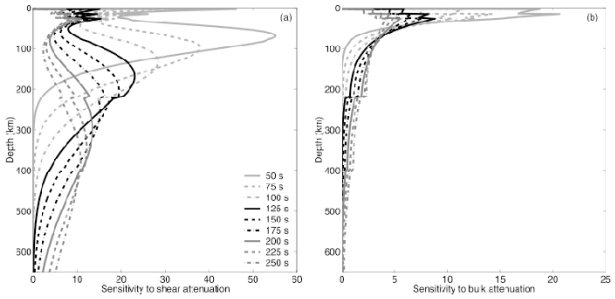

Figure 1. Rayleigh wave sensitivity kernels for the nine frequencies including in this study, calculated for PREM. (a) Sensitivity of the fundamental mode waves to shear attenuation. (b) Sensitivity of the fundamental mode waves to bulk attenuation. Note the different horizontal scales.

Another field to use surface waves is Earth's attenuation structure. Here, surface wave attenuation depends on both bulk and shear attenuation, Q_k and Q_mu.

Dalton, C.A., Ekstrom, G. and Dziewonski, A.M., The global attenuation structure of the upper mantle. J. Geophys. Res., VOL. 113, B09303, doi:10.1029/2007JB005429, 2008.

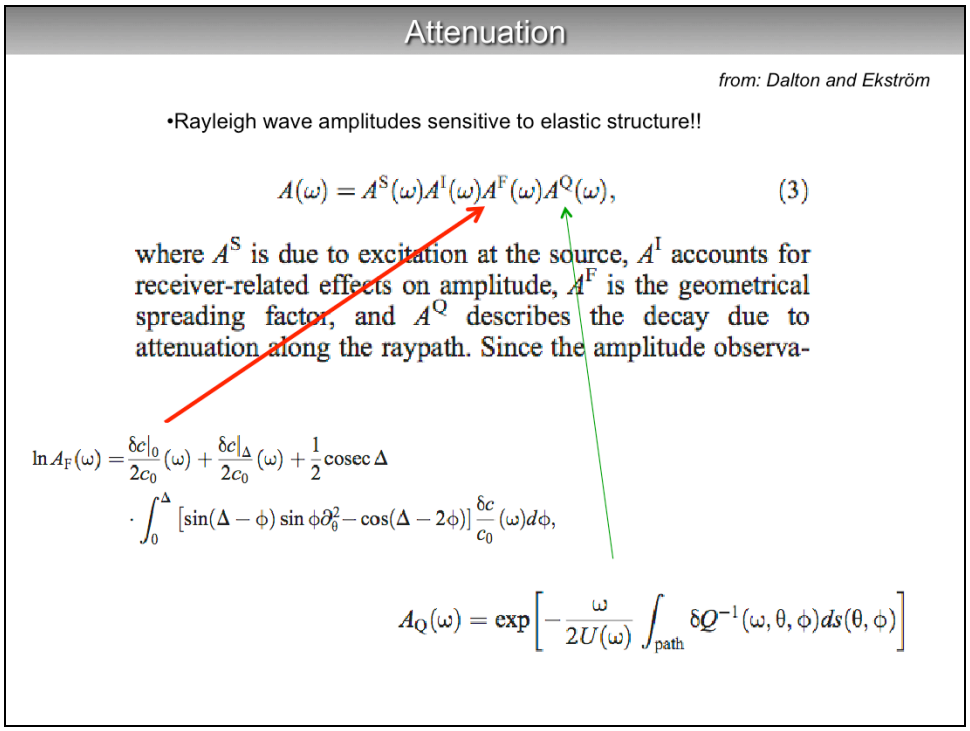

the complication of measuring surface wave amplitudes to infer attenuation is that amplitudes depend strongly on elastic structure through focusing and defocusing effects (A^F). In fact, the effect on amplitudes by Earth's elastic structure is much larger than that of attenuation structure (A^Q). To obtain attenuation structure, we therefore have to either correct amplitudes for effects from elastic structure before an inversion for attenuation structure. Or we invert jointly (using also phase data) for elastic and unelastic (attenuating) structure. Wodohhouse and Wong formulated linearized integral representations to describe the effects of elastic structure on amplitudes.

Attenuation

from: Dalton and Ekström

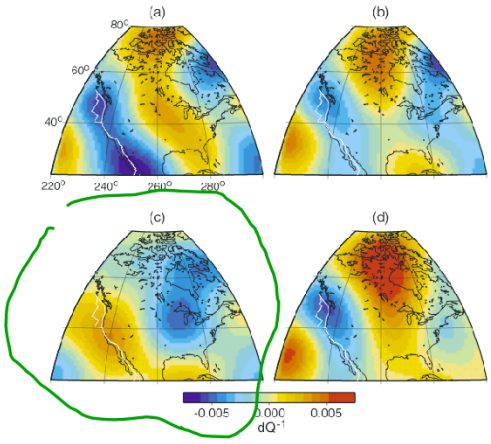

Figure 12. Same as Figure 11, but for 150-s Rayleigh waves and centered on North America. Q^{-1} is 0.00757 in PREM at 150 s.

in PREM. (a) The Q map that results when the amplitude data are inverted for attenuation maps only. No source, receiver, or focusing terms were included. (b) Map that results when the amplitude data are inverted for three quantities: attenuation maps, source factors, and receiver factors. (c) Our preferred Q map, which includes corrections for source and receiver uncertainty and elastic focusing. (d) The focusing Q map that results when a synthetic data set of focusing-predicted amplitudes is inverted for attenuation only.

a) A for Aq only
b) A for As, Aq and Ai
c) A for As, Aq, Ai and Af
d) synthetic test: Af for Aq

these panels demonstrate the importance of including the effects from elastic structure in the modeling.

Ignoring A^F (case a) results in wrong attenuation maps. c) is correct.

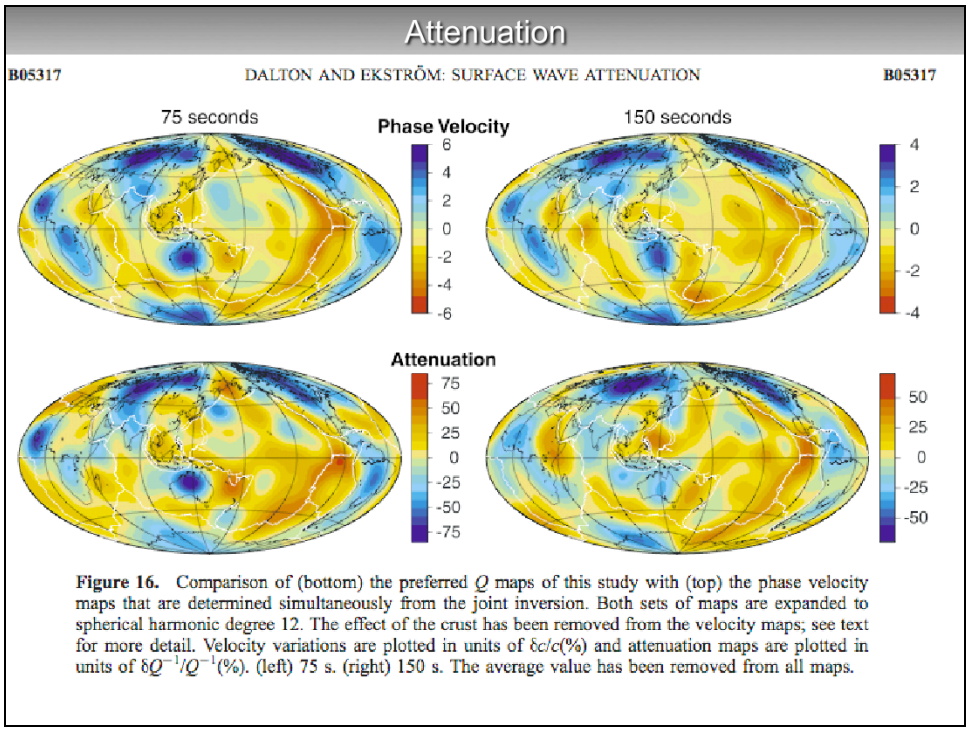

Figure 16. Comparison of (bottom) the preferred Q maps of this study with (top) the phase velocity maps that are determined simultaneously from the joint inversion. Both sets of maps are expanded to spherical harmonic degree 12. The effect of the crust has been removed from the velocity maps; see text for more detail. Velocity variations are plotted in units of $\delta c/c$(%) and attenuation maps are plotted in units of $\delta Q^{-1}/Q^{-1}$(%). (left) 75 s. (right) 150 s. The average value has been removed from all maps.

it turns out that, after accounting for focusing/defocusing effects on surface wave amplitudes, anelastic structure looks very similar to phase velocity maps (elastic structure), i.e. seismically fast regions are also less attenuating (e.g. continental cratons) while slower regions are more attenuating (e.g. mid-ocean ridges).